

1 **Early spring submarine discharge plumes fuel under-ice primary** 2 **production at a Svalbard tidewater glacier**

3

4 Tobias Reiner Vonnahme¹, Emma Persson¹, Ulrike Dietrich¹, Eva Hejdukova², Christine Dybwad¹, Josef
5 Elster³, Melissa Chierici^{4,5}, Rolf Gradinger¹

6 ¹ Department of Arctic and Marine Biology, UiT – The Arctic University of Norway, Tromsø, Norway

7 ² Department of Ecology, Faculty of Science, Charles University, Prague, Czech Republic

8 ³ University of South Bohemia, České Budějovice, and Institute of Botany ASCR, Třeboň, Czech Republic

9 ⁴ Institute of Marine Research, Tromsø, Norway

10 ⁵ University Centre in Svalbard (UNIS), Longyearbyen, Svalbard, Norway

11 *Correspondence to:* Tobias R. Vonnahme (T.r.vonnahme@gmail.com)

12 **Abstract.** Subglacial upwelling of nutrient rich bottom water ~~can~~ is known to sustain elevated summer primary production in
13 tidewater glacier influenced fjord systems. However, during the early spring season, the importance of subglacial upwelling
14 has not been considered yet ~~during the early spring season.~~ We hypothesized that submarine discharge under sea ice is present
15 in early spring and that its flux is sufficient to increase phytoplankton primary productivity. We evaluated the effects of the
16 submarine discharge on primary production in a seasonally fast ice covered Svalbard fjord (Billefjorden) influenced by a
17 tidewater outlet glacier in April/May 2019. We found clear evidence for subglacial discharge and upwelling. Although the
18 estimated bottom water entrainment factor (1.6) and total fluxes were lower than in summer studies, we still observed
19 substantial impact on the fjord ecosystem and primary production: at this time of the year. The subglacial ~~meltwater~~ discharge
20 leads to a salinity stratified surface layer and sea ice formation with low bulk salinity and permeability. The combination of
21 the stratified surface layer, a two-fold higher under-ice irradiance due to a thinner snow cover, and higher N and Si
22 concentrations at the glacier front supported two orders of magnitude higher phytoplankton primary production (42.6 mg C m⁻²
23 d⁻¹) compared to a marine reference site at the fast ice edge. The Reciprocal transplant experiments showed that nutrient
24 supply increased phytoplankton primary production by approximately 30 %. The brackish water sea ice at the glacier front
25 with its low bulk salinity contained a reduced brine volume, limiting the inhabitable ~~plae~~ brine channel space and nutrient
26 exchange with the underlying seawater compared to full marine sea ice. Microbial and algal communities were substantially
27 different in subglacial influenced water and sea ice compared to the marine reference site, sharing taxa with the subglacial
28 outflow water. We suggest that with climate change, the retreat of tidewater glaciers in early spring could lead to decreased
29 under-ice phytoplankton primary production, ~~while~~ In contrast, sea ice algae production and biomass may become increasingly
30 important, unless sea ice disappears before, in which case spring phytoplankton primary production may increase.

31

32

33

34 1 Introduction

35 Tidewater glacier fronts have recently been recognized as hotspots for marine production including top trophic levels, such as
36 marine mammals, birds and piscivorous fish (Lydersen et al., 2014, Meire et al., 2016b), but also primary producers (Meire et
37 al., 2016b; Hopwood et al., 2020). During summer, large amounts of freshwater are released below the glacier and entrain
38 nutrient rich bottom water, sediments and zooplankton during the rise to the surface (Meire et al., 2016a, Moon et al., 2018).
39 Together with katabatic winds pushing the surface water out of the fjords, submarine discharge creates a strong upwelling
40 effect (Meire et al., 2016a). The biological response to this upwelling will depend on the characteristics of the
41 ~~upwelling~~upwelled water. Primary production ~~and biomass~~ is typically low (e.g. $0.6 \pm 0.3 \text{ mg Chl } a \text{ m}^{-3}$, Halbach et al., 2019)
42 in direct proximity to the glacier front (~~within~~ hundreds of meters to kilometres ~~from the glacier front~~, Halbach et al., 2019)
43 due to high sediment loads of the plumes absorbing light, but ~~potentially~~ also due to lateral advection ~~and the time needed for~~
44 ~~algae growth~~ (Meire et al., 2016a,b; Halbach et al., 2019). The light absorbing effect of the plumes is highly dependent
45 on the glacial bedrock ~~type~~ (Halbach et al., 2019). ~~However, the~~The high nutrient concentrations supplied to the surface ~~can~~
46 increase summer primary production at some distance (~~more than~~ hundreds of meters to kilometres ~~away from the glacier~~
47 ~~front~~, Halbach et al., 2019) from the initial discharge event, once the sediments settled out ~~and algae had time to grow~~ (Meire
48 et al., 2016, Halbach et al., 2019). These tidewater upwelling effects have been described in a variety of different Arctic fjords
49 including deep glacier termini in western Greenland (Meire et al., 2016, 2016a,b), eastern Greenland (Cape et al., 2019), and
50 north-western Greenland (Kanna et al., 2018), but also in shallower fjords on Svalbard (Halbach et al., 2019). Due to the
51 challenges of Arctic ~~field work~~fieldwork in early spring and the difficulties of locating such an outflow, only few studies
52 investigated submarine discharge during that time window. The few studies available suggest ~~overall little~~overall low
53 discharge ~~flux~~ (e.g. Fransson et al., 2020; Schaffer et al., 2020) compared to summer values. ~~The~~However, the limited amount
54 of data makes the generalized quantification of ~~spring~~ subglacial outflow difficult. In addition, studies focusing on the potential
55 impacts of the early spring discharge on ~~both~~ sea ice and pelagic primary production are lacking.

56

57 In addition to submarine discharge at the grounding line, tidewater glacier related upwelling mechanisms can also be caused
58 by the melting of deep icebergs (Moon et al., 2018), or the melting of the glacier terminus in contact with warm seawater
59 (Moon et al., 2018, Sutherland et al., 2019). A seasonal study within an ~~e~~East Greenland fjord showed high melt rates of
60 icebergs throughout the year, while subglacial runoff had been detected as early as April, ~~but with~~ (Moon et al., 2018).
61 ~~However, freshwater inputs were generally~~ substantially higher ~~freshwater inputs~~ in summer (Moon et al., 2018). Glacier
62 terminus melt rates ~~occurring of basal ice~~ at the glacier-marine interface are low compared to the subglacial outflow ~~flux~~ but
63 can be present throughout the year (Chandler et al., 2013, Moon et al., 2018). In fact, Moon et al. (2018) found higher
64 ~~terminus basal iceberg~~ melt rates below 200 m in winter ~~than in~~compared to summer. ~~The freshwater flux from these icebergs~~
65 ~~exceeds summer river runoff and reaches values of early summer (June-July) subglacial discharge~~ (Moon et al., 2018), which
66 may allow winter upwelling. Submarine glacier ~~termina~~termini on Svalbard occur typically at shallower water ~~depth~~depths

67 than on Greenland and deep ~~terminus~~basal melt at the glacier terminus (below 200 m) and iceberg induced upwelling are less
68 important (Dowdeswell, 1989). However, subglacial outflows can persist through winter and into spring through the release
69 of subglacial meltwater stored from the previous melt season (Hodgkins, 1997). Hodgkins (1997) described the release of
70 subglacial meltwater stored from the previous summer ~~and~~to fall melt season ~~as observed in several~~from various Svalbard
71 glaciers, ~~including cold based glaciers (Hodgkins, 1997)~~. Winter drainage occurred mostly periodically during events of ice-
72 dam breakage in the subglacial drainage system. During the storage period, the meltwater ~~can~~changes its chemical
73 composition. ~~For example, During~~ prolonged contact with silicon-rich bedrock ~~increased the,~~ the meltwater becomes enriched
74 in the macronutrient silicate ~~concentrations~~ (Hodgkins, 1997). ~~Additionally, During~~ freezing of ~~some of~~ the meltwater ~~leads,~~
75 solutes are expelled leading to higher ion concentrations in the ~~remaining~~ liquid fraction (Hodgkins, 1997). Under polythermal
76 glaciers, various ~~additional~~other mechanisms such as constant freshwater supply from groundwater, and basal ice melt via
77 geothermal heat, pressure, or frictional dissipation can also ~~contribute to~~be a continuous, but low flux meltwater source in
78 winter and spring (Schoof et al., 2014). ~~Sediment inputs into the fjord~~ during this time of the year are low with peaks deeper
79 in the water column, indicating limited impacts on surface primary production (Moskalik et al., 2018). While studies on glacial
80 discharge in winter and spring are limited to oceanographic observations (Fransson et al., 2020, Schaffer et al., 2020), the
81 biological effects on e.g. primary production have been neglected (Chandler et al., 2013, Moon et al., 2018). We hypothesize
82 that ~~subglacial~~submarine discharge can lead to significantly increased primary production, due to upwelling of nutrient-rich
83 deeper water or through its own nutrient load, especially towards the end of the spring bloom. ~~We suggest that during this~~At
84 the same ~~time~~time, considerably less light absorbing sediments are entrapped due to lower upwelling fluxes-compared to the
85 summer ~~situation~~ (Moskalik et al., 2018).

86
87 ~~With the return of the sunlight after the polar night, Arctic~~After light becomes available in spring, ice algae and phytoplankton
88 may start forming blooms ~~sustained~~fuelled by ~~the~~nutrients supplied via winter mixing-~~replenished nutrients~~ with different
89 onsets in different parts of the Arctic. The blooms are typically terminated by limitation of macronutrients, ~~mainly~~either nitrate
90 or silicate (Leu et al., 2015). We suggest that in the absence of wind induced mixing, due to the seasonal presence of a fast ice
91 cover in spring, submarine discharge of glacial meltwater can directly (nutrient and ion enrichment over the subglacial storage
92 period) or indirectly (upwelling) be a significant source of inorganic ~~nutrient increasing~~nutrients. We suggest that these
93 nutrients can significantly increase primary production in front of tidewater glaciers compared to similar fjords without these
94 glaciers. ~~Especially~~ especially after nutrients supplied via winter mixing are ~~incorporated into algal biomass~~used up (Leu et
95 al., 2015) ~~this additional nutrient source may become important. Evaluating this process is also relevant as~~. With climate
96 change ~~will substantially change,~~ these dynamics are expected to change substantially (e.g. Błaszczyk et al., 2009, Holmes et
97 al., 2019). Higher glacial melt rates and earlier ~~runoffs~~runoff may initially increase tidewater glacier induced upwelling, due
98 to increased subglacial runoff (Amundson and Carroll, 2018). However, their retreat and transformation into shallower
99 tidewater glacier termini may lead to less pronounced upwelling, unless the shallower grounding line is compensated by the
100 increased runoff (Amundson and Carroll, 2018). Eventually, the tidewater glaciers transform into land terminating glaciers,

101 where wind induced mixing is still possible, but submarine discharge is eliminated (Amundson and Carroll, 2018) – potentially
102 reducing primary production.

103

104 Due to high inputs of freshwater in the autumn preceding the onset of sea ice formation, tidewater glacier influenced fjords are
105 often sea ice covered in spring, mainly by coastal fast ice. Within the sea ice, ice algae start growing, once sufficient light
106 penetrates the snow and ice layers, ~~ice algae start growing within sea ice~~ between March and April, depending on latitude and
107 local ice conditions (Leu et al., 2015). While the beginning of the ice algal blooms is typically related to light, the magnitude
108 depends on the initial nutrient ~~concentration~~concentrations and advection of nutrient-rich seawater from the water column into
109 the brine channel network (Gradinger, 2009). Thus, early spring ~~subglacial~~subglacially induced upwelling has the strong
110 potential to extend the duration and increase the magnitude of the ice algal blooms. Similar control mechanisms apply to
111 phytoplankton bloom formation and duration. ~~Phytoplankton growth under sea ice is often light limited, and under~~Under-ice
112 phytoplankton blooms ~~are thought to be light limited if the ice is snow covered and blooms~~ have mostly been described in
113 areas with ~~increased under ice light intensities due to e.g. the a~~ lack of snow cover (e.g. melt ponds, after rain events, Fortier
114 et al., 2002, Arrigo et al., 2014) or at the ice edge related to -wind-induced Ekman upwelling (Mundy et al., 2009). On Svalbard,
115 low precipitation rates and strong katabatic winds (Esau & Repina, 2012) often limit snow accumulation also on the fast ice
116 near glacier fronts (Braaten, 1997), potentially allowing enough light for under-ice phytoplankton blooms to occur. ~~We also~~
117 ~~suggest that the unique sea ice features could increase the under ice light intensity. Sea ice formed from brackish water has a~~
118 ~~low bulk salinity, brine volume fraction and permeability (Golden et al., 1998) and resulting low total ice algal biomass as~~
119 ~~observed e.g. After~~in the Baltic Sea (Haecky & Andersson, 1999). This lower algal biomass will reduce ice algal light
120 ~~absorption allowing more light to reach the under ice phytoplankton. With~~ sufficient light reaches the water column, typically
121 a diatom dominated ~~phytoplankton~~-bloom starts along the receding ice edge or even below the sea ice (e.g. Hodal et al., 2012;
122 Lowry et al., 2017). Once silicate becomes limiting for diatom growth, other taxa like *Phaeocystis pouchetii* dominate the next
123 stage of the seasonal succession (von Quillfeldt, 2000). ~~These algal~~This succession pattern ~~in ice and water column~~ can be
124 significantly influenced by tidewater glacier induced spring upwelling. Sea ice formed from brackish water has relatively low
125 bulk salinity, low brine volume, and low total ice algal biomass as observed e.g. in the Baltic Sea (Haecky & Andersson, 1999).
126 Sea ice with reduced bulk salinity has a reduced permeability compared to more saline ice at identical temperatures (Golden
127 et al., 1998). Brackish ice conditions with low algal biomass will reduce light absorption allowing more light to reach the water
128 column potentially fuelling under-ice phytoplankton blooms. We suggest that ~~higher nutrient levels supplied via even though~~
129 ~~subglacial upwelling of low total flux is diminished in the spring, compared to the summer,~~ in the absence of wind mixing-, the
130 enriched nutrient concentrations may enhance algal growth- at this time of year.

131

132 We used the natural conditions in a Svalbard fjord as a model system contrasting the biological response at two glacier fronts
133 ~~with only. Only~~ one of the glacier ~~front supplying submarine~~fronts supplies submarine freshwater discharge during the
134 winter/spring (early spring) transition period while a fast ice cover was present. In contrast, the other glacier front is mostly

135 land-terminating. The aim of the study was to investigate the effect of the glacier terminus, and subglacial outflow related
136 upwelling on the light and nutrient regime in the fjord and thereby on early spring primary productivity and algae community
137 structures both in and under the sea ice. We hypothesized that; 1) submarine discharge throughout winter and spring supplies
138 nutrient rich glacial meltwater and upwelling of marine bottom water to the surface, 2) submarine discharge increases primary
139 production near the glacier front (< 500 m), 3) biomass of sea ice algae is lower at glacier fronts as a result of low permeability
140 sea ice limiting nutrient exchange and inhabitable space.

141 2 Methods

142 2.1 Field work and physical properties

143 Fieldwork was conducted on Svalbard in Billefjorden (Fig. 1) between 22nd of April and 5th of May 2019, when most ~~of the~~
144 samples were collected. For comparison, ~~additional~~some samples had been already taken in April 2018 (seawater, sea ice, and
145 subglacial outflow water for DNA analyses) and July 2018 (glacier ice and supraglacial runoff). Billefjorden is fed by a few
146 streams, rivers and the tidewater glacier Nordenskiöldbreen and is partly fast ice covered from January to June.
147 Nordenskiöldbreen has an estimated grounding depth of 20 m at its southern margin (personal observation). Tidal currents are
148 very slow with under 0.1 cm s⁻¹, which translates to advection below 22 m per tidal cycle (Kowalik et al., 2015). Katabatic
149 winds can be strong due to several glaciers and valleys leading into the fjord system (Láska et al., 2012). Together with low
150 precipitation, this leads to a thin snow depth on the sea ice. Bare sea ice spots are often present in the sea ice season (personal
151 observations). The fjord is separated from Isfjorden, a larger fjord connected to the West Spitsbergen current, by a shallow
152 approximately 30 to 40 m ~~deep~~-sill (Norwegian Polar Institute, 2020) making Billefjorden an Arctic fjord with limited impacts
153 of Atlantic water inflows. This character is shown in water masses, circulation patterns and animal communities including the
154 presence of polar cod (Maes, 2017, Skogseth et al., 2020).

155 Samples were taken at three stations: 1) at the fast ice edge (IE) – a full marine reference station (78°39'09N, 16°34'01E); 2)
156 at the southern site of the ocean terminated glacier terminus (SG) (approx. 20 m water depth) with freshwater outflow observed
157 during the sampling period (78°39'03N, 16°56'44E) and; 3) at the northern site of the glacier terminus (NG) with no clear
158 freshwater outflow observed and a mostly land-terminating glacier front (78°39'40N, 16°56'19E).

159 Snow depth and sea ice thickness around the sampling area were measured with a ruler. Sea ice and glacier ice samples were
160 taken with a Mark II ice corer with an inner diameter of 9 cm (Kovacs Enterprise, Roseburg, OR, USA). Temperature of each
161 ice core was measured immediately by inserting a temperature probe (TD20, VWR, Radnor, PA, USA) into 3 mm thick pre-
162 drilled holes. For further measurements the ice cores were sectioned into the following sections: 0–3 cm, 3–10 cm and
163 thereafter in 20 cm long pieces from the bottom to the top, packed in sterile bags (Whirl-Pak™, Madison, WI, USA) and left
164 to melt at about 4–15 °C for about 24–48 h in the dark. Sections for chlorophyll *a* (Chl) measurements, DNA extractions, and
165 algae and bacteria counts were melted in 50 % vol/vol sterile filtered (0.2 µm Sterivex filter, Sigma-Aldrich, St. Louis, MO,
166 USA) seawater to avoid osmotic shock of cells (Garrison and Buck, 1986), while no seawater was added to the sections for

167 salinity and nutrient measurements. Salinity was measured immediately after melting using a conductivity sensor (YSI Pro 30,
168 YSI, USA). Brine salinity and brine volume fractions were calculated after Cox et al. (1983) for sea ice temperatures below -
169 2 °C and after Leppäranta and Manninen (1988) for sea ice temperatures above -2 °C.
170 Samples of under-ice water were taken using a pooter (Southwood and Henderson, 2000) connected to a hand-held vacuum
171 pump (PFL050010, Scientific & Chemical Supplies Ltd., UK). Deeper water at 1 m, 15 m, 25 m depths and bottom water at
172 the IE station were taken with a water sampler (Ruttner sampler, 2 L capacity, Hydro-Bios, Germany). Glacial outflow water
173 was sampled in April 2018 close to the SG station using sterile Whirl-Pak™ bags. No outflow water was found around the NG
174 station. Cryoconite hole water (avoiding any sediment) was sampled in July 2018 with a pooter on sites known to differ in
175 their biogeochemical settings (Nordenskiöldbreen main cryoconite site (NC), and Nordenskiöldbreen near Retrettøya (NR)
176 sites characterized by Vonnahme et al., 2016). One-metre long glacier surface ice samples were taken with the Mark II ice
177 corer at the southern side of the glacier on the NC site.
178 CTD profiles were taken at each station by a CastAway™ (SonTek/-Xylem, San Diego, CA, USA). At the SG station an
179 additional CTD profile was taken with a SAIV CTD SD208 (SAIV, Lakselv, Norway) including turbidity and fluorescence
180 sensors. Unfortunately, readings at the other stations failed due to sensor freezing at low air temperatures. Surface light data
181 were obtained from the photosynthetic active radiation (PAR) sensor of the ASW 1 weather station in Petuniabukta (23 m
182 a.s.l), operated by the University of South Bohemia (Láska et al., 2012; Ambrožová and Láska, 2017).
183 During the sampling days, Billefjorden ~~and Adventdalen were~~was overcast. The light regime under the ice was calculated after
184 Masicotte et al. (2018) with a snow albedo of 0.78, a snow attenuation coefficient of 15 m⁻¹ (Mundy et al., 2005), ice attenuation
185 coefficients of 5.6 m⁻¹ for the upper 15 cm and 0.6 m⁻¹ below (Perovich et al., 1998). For sea ice algae, an absorption coefficient
186 of 0.0025 m² (mg⁻¹ Chl)⁻¹ was used. The fraction of fjord water vs subglacial meltwater for the water samples was calculated
187 assuming linear mixing (Equations 1-2) of the two salinities (glacial meltwater salinity = 0 PSU, average seawater salinity at
188 IE=34.7 ± 0.03 standard deviation), since no other water masses in regard to temperature or salinity signature were present
189 (Table 1). The variability of the IE seawater salinity leads to a small (~~0~~<1%) uncertainty in the estimated value of the relative
190 contributions of sea water vs subglacial meltwater.

191 2.2 Chemical properties

192 Nutrient samples of water and melted sea ice and glacier ice were sterile filtered as described above, stored in acid washed
193 (rinsed in 5 % vol/vol HCl) and MQ rinsed 50 ml falcon tubes and kept at -20 °C until processing. Total alkalinity (TA),
194 Dissolved inorganic carbon (DIC), and pH samples were sampled in 500 ml borosilicate glass bottles avoiding air
195 contamination and fixed within 24 h with 2 % (~~fin. conc.~~final conc.) HgCl₂ and stored at 4 °C until processing.

196 Nutrients were measured in triplicates using standard colorimetric methods with a nutrient autoanalyser (QuAAtro 39, SEAL
197 Analytical, Germany) using the instrument protocols: Q-068-05 Rev. 12 for nitrate (detection limit = 0.02 µmol L⁻¹), Q-068-
198 05 Rev. 12 for nitrite (detection limit = 0.02 µmol L⁻¹), Q-066-05 Rev. 5 for silicate (detection limit = 0.07 µmol L⁻¹), and Q-
199 064-05 Rev. 8 for phosphate (detection limit = 0.01 µmol L⁻¹). The data were analysed using the software AACE v5.48.3

200 (SEAL Analytical, Germany). Reference seawater (Ocean Scientific International Ltd., United Kingdom) was used as blanks
201 for calibrating the nutrient analyser. The maximum differences between the measured triplicates were $0.1 \mu\text{mol L}^{-1}$ for silicate
202 and nitrate and $0.05 \mu\text{mol L}^{-1}$ for nitrite and phosphate. Concentrations of nitrate and nitrite (NO_x) were used to estimate the
203 fraction of bottom water reaching the surface at SG assuming linear mixing of subglacial meltwater, bottom water (at station
204 IE) and surface water concentration using the NO_x concentration measured at IE and the subglacial meltwater (Table 1). The
205 calculations for these mixing estimates are given in the appendix- [\(Equations 3-6\)](#).
206 DIC and TA were analyzed within 6 months after sampling as described by Jones et al. (2019) and Dickson et al. (2007). DIC
207 was measured on a Versatile Instrument for the Determination of Titration carbonate (VINDTA 3C, Marianda, Germany),
208 following acidification, gas extraction, coulometric titration, and photometry. TA was measured with potentiometric
209 ~~titration~~ [titrations](#) in a closed cell on VINDTA Versatile INstrument for the Determination of Titration Alkalinity, VINDTA
210 3S, Marianda, Germany). Precision and accuracy was ensured via measurements of Certified Reference Materials (CRM,
211 obtained from Dickson, Scripps Institution of Oceanography, USA). Triplicate analyses on CRM samples showed mean
212 standard deviations below $\pm 1 \mu\text{mol kg}^{-1}$ for DIC and [TAAT](#).

213 **2.3 Biomass and communities**

214 For determination of algal pigment concentrations, about 500 ml sea water or melted sea ice were filtered onto GF/F filter
215 (Whatman plc, Maidstone, UK) in triplicates using a vacuum pump (max 200 mbar vacuum) before storing the filter in the
216 dark at -20°C . Water and melted sea ice for DNA samples were filtered onto Sterivex filter ($0.2 \mu\text{m}$ pore size) using a peristaltic
217 pump and stored at -20°C until extraction. Algae were sampled in two ways; 1) a phytoplankton net ($10 \mu\text{m}$ mesh size) was
218 pulled up from 25 m and the samples fixed in 2 % (final conc.) neutral Lugol and stored at 4°C in brown borosilicate glass
219 bottles before processing; and 2) water or melted sea ice was fixed and stored directly as described above. For later bacteria
220 abundance estimation, 25 ml of water was fixed with 2 % (final ~~con~~ [conc.](#)) formaldehyde for 24–48 h at 4°C before filtering
221 onto $0.2 \mu\text{m}$ polycarbonate filters (Isopore™, Merck, US) and washing with filtered seawater and 100 % ethanol before
222 freezing at -20°C .

223 Algal pigments (Chl [a](#), phaeophytin) were extracted in 5 ml 96 % ethanol at 4°C for 24 h in the dark. The extracts were
224 measured on a Turner Trilogy AU-10 fluorometer (Turner Designs, 2019) before and after acidification with a drop of 5 %
225 HCl. 96 % ethanol was used as a blank and the fluorometer was calibrated using a chlorophyll standard (Sigma S6144). For
226 estimations of algae derived carbon, a conversion factor of $30 \text{ g C (g Chl)}^{-1}$ was applied (Cloern et al., 1995). The maximum
227 differences (max-min) between the measured triplicates were under $0.05 \mu\text{g Chl L}^{-1}$ unless stated otherwise.

228 DNA was isolated from the Sterivex filter cut out of the cartridge using sterile pliers and scalpels, using the DNeasy®
229 PowerSoil® Kit following the kit instructions with a few modifications. Solution C1 was replaced with $600 \mu\text{L}$
230 Phenol:Chloroform:Isoamyl Alcohol 25:24:1 and washing with C2 and C3 was replaced with two washing steps using $850 \mu\text{L}$
231 chloroform. Before the last centrifugation step, the column was incubated at 55°C for 5 min to increase the yield. For microbial
232 community composition analysis, we amplified the V4 region of a ca. 292 bp fragment of the 16S rRNA gene using the primers

233 (515F, GTGCCAGCMGCCGCGGTAA and 806R, GGAATCHVGGGTWTCTAAT, assessed by Parada et al., 2016). For
234 eukaryotic community composition analyses, we amplified the V7 region of ca 100-110 bp fragments of the 18S rRNA gene
235 using the primers (Forward 5'-TTTGTCTGSTTAATTSCG-3' and Reverse 5'-GCAATAACAGGTCTGTG-3', assessed by
236 Guardiola et al., 2015). The Illumina MiSeq PE library was prepared after Wangenstein et al. (2018).
237 For qualitative counting of algal communities, the phytoplankton net and bottom sea-ice samples were counted under an
238 inverted microscope (Zeiss Primovert, Carl Zeiss AG, Germany) with 10x40 magnification. For quantitative counts, 10-50 ml
239 of the fixed water samples were settled in an Utermöhl chamber (Utermöhl, 1958) and counted. Algae were identified using
240 identification literature by Tomas (1997), and Thronsen et al. (2007). For bacteria abundance estimates, bacteria on
241 polycarbonate filter samples were stained with DAPI (4,6-diamidino-2-phenylindole) as described by Porter and Feig (1980),
242 incubating the filter in 30 µl DAPI (1 µg ml⁻¹) for 5 min in the dark before washing with MQ and ethanol and embedding in
243 Citifluor:Vectashield (4:1) onto a microscopic slide. The stained bacteria were counted using an epifluorescence microscope
244 (Leica DM LB2, Leica Microsystems, Germany) under UV light at 10x100 magnification. At least 10 grids or 200 cells were
245 counted. The community structure of the phytoplankton net haul was used for estimating the contribution of sea ice algae to
246 the settling community based on typical Arctic phytoplankton (Von Quillfeldt, 2000) and sea ice algal species (von Quillfeldt
247 et al., 2003) described in literature.

248 **2.4 In situ measurements and incubations**

249 Vertical algal pigment fluxes were measured using custom made (Faculty of Science, Charles University, Prague, Czech
250 Republic) short-term sediment traps (6.2 cm inner diameter, 44.5 cm height) at 1 m, 15 m, and 25 m under the sea ice anchored
251 to the ice at SG and IE, as described by Wiedmann et al. (2016). Sediment traps were left for 24 h at the SG station and 37 h
252 at the IE station. After recovery, samples for algal pigments were taken, fixed and analysed as described above. Vertical export
253 ~~was~~ fluxes were calculated as described in equation 7.

254 Primary production (PP) was measured based on ¹⁴C-DIC incorporation. Samples were incubated *in situ* in 100 ml polyethylene
255 bottles attached to the rig of the sediment trap giving identical incubation times. Seawater or bottom sea ice melted in filtered
256 seawater (ca 20 °C initial temperature to ensure fast ice melt) on site were incubated with ¹⁴C sodium bicarbonate at final
257 concentration of 1 µCi ml⁻¹ (PerkinElmer Inc., Waltham, USA). PP samples were incubated in triplicates for each treatment
258 with two dark controls for the same times as the sediment traps. Samples were filtered onto precombusted Whatman GF/F
259 filters (max 200 mbar vacuum) and acidified with a drop of 37 % fuming HCl for 24 h for removing remaining inorganic
260 carbon. The samples were measured in the Ultima Gold™ Scintillation cocktail on a liquid scintillation counter (PerkinElmer
261 Inc., Waltham, USA, Tri-Carb 2900TR) and PP was calculated after Parsons et al., (1984). Dark carbon fixation (DCF) rates
262 were used to estimate bacterial biomass production using a conversion factor of 190 mol POC (mol CO₂)⁻¹ fixed (Molari et al.,
263 2013).

264 For testing the effect of the water chemistry on phytoplankton growth, we designed a reciprocal transplant ~~primary production~~
265 experiment where the phytoplankton communities at SG and IE (1 m and 15 m) ~~each~~ were transplanted into the sterile filtered

266 water of both SG and IE. 50 ml of the water containing the ~~respective original~~ phytoplankton ~~community communities of SG~~
267 ~~or IE~~ were transferred into 50 ml sterile filtered (0.2 µm) seawater of SG or IE ~~each~~ in 100 ml polyethylene bottles. The bottles
268 ~~with IE communities~~ were then incubated ~~in situ~~ under the ice at the ~~original depth~~ IE station and ~~primary production measured~~
269 ~~as described above~~ the SG communities under the ice at the SG station. The aim of the experiment is to test if water chemistry
270 alone is sufficient to increase primary production, or if ~~differences in algal~~ the different communities, light regimes, or
271 temperatures are more important. These samples were incubated and processed together with the other PP incubations at the
272 ~~adequate~~ respective depths as described above.

273 2.5 Statistics and bioinformatics

274 Silicate, phosphate and NO_x concentrations were plotted against salinities and ~~correlation were~~ tested for correlations via linear
275 regression analysis using the lm function in R (R Core Team, Vienna, Austria). P values were corrected for multiple testing
276 using the false discovery rate. Since the primary production estimates of the reciprocal transplant experiments were not
277 normally distributed, came from a nested design, and had heterogeneous variance, a robust nested Analysis of variance
278 (ANOVA) was performed to test for significant treatment effects of incubation water with water depth as nested variable. The
279 map (Fig. 1) was created in R using the PlotSvalbard v0.9.2 package (Vihtakari, 2020). The Svalbard basemap was retrieved
280 from the Norwegian Polar institute (2020, CC BY 4.0 license), the pan-Arctic map was retrieved from Natural Earth (2020,
281 CC Public domain license), and the bathymetric map was retrieved from the Norwegian mapping authority (Kartverket, 2020,
282 CC BY 4.0 license).

283 16S sequences were analysed using a pipeline modified after Atienza et al. (2020) based on OBITools v1.01.22 (Boyer et al.,
284 2014). The raw reads were demultiplexed and trimmed to a median phred quality score minimum of 40 and sequence lengths
285 between 215 bp and 299 bp (16S rRNA) or between 90 bp and 150 bp (18S rRNA) and merged. Chimaeras were removed
286 using uchime with a minimum score of 0.9. The remaining merged sequences were clustered using swarm (Mahe et al., 2014).
287 16S swarms were classified using the RDP classifier (Wang et al., 2007) and 18S swarms using the sina aligner (Pruesse et
288 al., 2012) with the silva SSU 138.1 database (Quast et al., 2012). Further multivariate analyses were done in R using the vegan
289 package. The non-metric multidimensional scaling (NMDS) plots are based on Bray-Curtis dissimilarities of square root
290 transformed and double Wisconsin standardized OTU tables and were used to visualize differences between groups (brackish
291 water at SG – Fjord water, sea ice – seawater). Analysis of Similarities (ANOSIM) were done to test for differences of the
292 communities between the groups (999 permutations, Bray-Curtis dissimilarities).

293 3 Results

294 3.1 Physical parameters

295 The physical conditions of sea ice (temperature T/bulk salinity S, Fig. 2a,-b) and surface water (uppermost 4 m under the sea
296 ice, T and S, Fig. 2c,d) at the freshwater inflow impacted site SG differed substantially from NG and IE. The sea ice and the

297 upper 4 m under the sea ice had consistently lower salinities (<8 PSU) and higher temperatures (-0.4 °C to -0.2 °C) at SG
298 compared to NG and IE and also compared to the deeper water masses at SG (salinity > 34.6 PSU, temperature < -1.4 °C)(Fig.
299 2c,d). Sea ice melt was unlikely because the measured water temperatures and sea ice temperatures were below the freezing
300 point considering the sea ice bulk salinity. The water column at SG was highly stratified with a low salinity 4 m thick layer
301 under the sea ice, separated by a sharp ca 1 m thick pycnocline (Fig. 2c,d). In contrast, the water column at IE was fully mixed
302 and at NG only a minor salinity drop from 34.6 to 33.6 PSU occurred within the the upper 50 cm under the sea ice (Fig. 2c,d).
303 Sea ice temperature and salinity showed similar variations between the three sites with SG ice having lower salinities and
304 higher temperatures relative to sea ice at the other stations (Fig. 2a,b). At SG, bulk salinities were mostly below 0.7 PSU and
305 calculated brine salinities below 14 PSU, except for the uppermost ~~40-20~~ cm where bulk salinities reached around 1.~~75~~ PSU
306 and a brine salinity of 32 PSU (Fig. 2). This resulted in very low brine volume fractions below 5 %, except for the lowermost
307 10 cm with brine volume fractions up to 9 % (Supplementary table S1). At IE and NG, bulk salinities are mostly above 5 PSU
308 (>40 PSU brine salinity) and temperatures were below -0.4 °C, which led to brine volume fractions above 6 % in all samples
309 and above 10 % in the bottom 30 cm.

310 The homogenous temperature and salinity water column profiles at IE and NG stations indicate the presence of only one water
311 mass (Local Arctic water, Skogseth et al., 2020). The only additional water mass was subglacial meltwater (salinity of 0 PSU)
312 mixed into the surface layer of SG. Applying a simple mixing model based on the two salinities (IE= 34.~~76~~ PSU, Glacier= 0
313 PSU) ~~provide~~provided an estimation of the fraction of glacially derived water in the surface layer of ca. 85 % in the uppermost
314 2 m under the sea ice, before decreasing to 0 % at 4 m under the sea ice below the strong halocline. The water sample taken 1
315 m under the sea ice had a fraction of 32 % glacial meltwater (Table 1). For NG, glacial derived water contributed only 3 % in
316 the first 50 cm under the sea ice.

317 The SG station was 33 m deep and about 180 m away from the glacier front. The sea ice was 1.33 m thick and covered by 3
318 cm of snow. The ice appeared clear with some minor sediment and air bubble inclusions and missed a skeletal bottom layer.
319 In the water column, a higher potential sediment load was observed as a turbidity peak at the halocline (Fig. 3). Direct evidence
320 of subglacial outflow had been observed at the southern site of the glacier in form of icing and liquid water flowing onto the
321 sea ice in April 2018, April 2019 and October 2019 (Fig. S4), but this form of subglacial outflow froze before reaching the
322 fjord, which was additionally blocked by impermeable sea ice. The sea ice temperature was between -0.4 °C at the bottom and
323 -1.7 °C at the top (Fig. 2b).

324 NG was 27 m deep and about 360 m away from the glacier front. The sea ice was thinner (0.92 m) and the snow cover thicker
325 (6 cm) compared to SG. The ice had a well developed skeletal layer at the bottom with brown coloration due to algal biomass.
326 The ice temperature ranged between -2 °C at the bottom to -2.7 °C at the top (Fig. 2b). The IE station was about 75 m deep
327 and 50 m away from the ice edge. The sea ice was thinnest (0.79 m) and the snow cover thickest (10 cm). Sea ice temperatures
328 were coldest ranging from -2.2 °C at the bottom to -3.1 °C on the top (Fig. 2b). Loosely floating ice algae aggregates were
329 present in the water directly under the ice. The recorded surface PAR irradiance were similar during the primary production
330 incubation times at SG and IE (SG: average=305 $\mu\text{E m}^{-2} \text{ s}^{-1}$, min=13 $\mu\text{E m}^{-2} \text{ s}^{-1}$, max=789 $\mu\text{E m}^{-2} \text{ s}^{-1}$; IE: average=341 $\mu\text{E m}^{-2}$

331 s^{-1} , $\min=37 \mu E m^{-2} s^{-1}$, $\max=909 \mu E m^{-2} s^{-1}$). Using published attenuation coefficients irradiance directly under the ice was 5
332 $\mu E m^{-2} s^{-1}$ at IE and ~~higher at SG~~-with $9 \mu E m^{-2} s^{-1}$ higher at SG due to the thinner snow cover.

333 3.2 Nutrient variability in sea ice and water

334 Subglacial outflow water and glacial ice had relatively low nutrient ~~concentrations (levels (in~~ glacial ice: $Si(OH)_4 < 0.3 \mu mol$
335 L^{-1} , $NO_x < 0.9 \mu mol L^{-1}$, $PO_4 < 0.875 \mu mol L^{-1}$, in outflow: $Si(OH)_4 < 1.5- 2.0 \mu mol L^{-1}$, $NO_x 1.8- 2.3 \mu mol L^{-1}$, $PO_4 < 0.1$
336 $\mu mol L^{-1}$).~~The), but the~~ nutrient concentrations in subglacial outflow water were higher than in most sea ice samples and the
337 ~~nutrient~~-depleted surface water (1 m under the sea ice) at ~~station~~the IE. Nutrient concentrations in the fjord were highest in the
338 bottom water ($4.0- 4.5 \mu mol L^{-1} Si(OH)_4$, $9.1- 9.6 \mu mol L^{-1} NO_x$, $0.7-0.8 \mu mol L^{-1} PO_4$) and depleted at the surface and in the
339 sea ice with the exception of the under-ice water (UIW, 0- 1 cm under the sea ice) of SG, where $NO_x (10 \mu mol L^{-1})$ and silicate
340 ($19 \mu mol L^{-1}$) levels were exceptionally high (Fig. 4). We cannot exclude anomalies or sampling artifacts to be responsible for
341 the high ~~values supported only from triplicate measurement of one sample, and therefor decided to use UIW values, and~~
342 therefore used the values measured 1 m under the sea ice for further calculations in this manuscript as surface water reference.
343 SG had overall higher levels of silicate and NO_x compared to the IE at both 1 m below the sea ice (~~by~~-factors of 3 for $Si(OH)_4$
344 and 2 for NO_x) and bottom ice (~~by~~-factor of 18 for $Si(OH)_4$ and 3 for NO_x compared to IE bottom ice) (Fig. 4). Silicate
345 concentrations deeper in the water column were similar at all the stations with values of ca $4 \mu mol L^{-1}$ -. Close to the surface
346 silicate was reduced to $1.6 \mu mol L^{-1}$ at 1 m at the IE, while it stayed at $4.3 \mu mol L^{-1}$ at SG (Fig. 4a). In the water column, NO_x
347 and phosphate gradients were similar between the sites. However in sea ice, NO_x concentrations were more than two times
348 higher at SG than at the IE. In the bottom 30 cm of sea ice all nutrients had higher concentrations at SG, except for phosphate,
349 which was depleted in the bottom 3 cm of SG, but not in the bottom of IE sea ice. In the ice interior ~~inat~~ 50- 70 cm distance
350 from the ice bottom, also the other nutrients were depleted at SG, before rising slightly towards the surface of the ice. N:P
351 ratios were generally highest at SG with values above 40, exceeding Redfield ratios in the surface water and sea ice. N:P ratios
352 at the IE were below Redfield in the entire water column and bottom sea ice with values ranging from 10 to 13. A slight
353 increase in NO_x was observed at the sea ice-atmosphere interface at NG and SG.

354 Nutrient versus salinity profiles can give indications of the endmembers (sources) of the nutrients (Fig. 5) ~~based on~~with a linear
355 correlation indicating being indicative of conservative mixing. A positive correlation indicates higher concentrations of the
356 nutrients ~~in of~~ the saline Atlantic water endmember, while a negative correlation points to a higher concentration in the fresh
357 glacial meltwater endmember. Biological uptake and remineralisation could weaken or eliminate the correlation, indicating
358 non-conservative mixing. In the water column at NG and IE, silicate ($R^2=0.66$, $p=0.008$), NO_x ($R^2=0.62$, $p=0.01$) and
359 phosphate ($R^2=0.69$, $p=0.005$) showed conservative positive mixing patterns with higher contributions of Atlantic ~~Water~~water
360 (Fig. 5a-c). ~~At~~-SG showed a negative correlation for silicate ~~was negatively correlated to salinity~~ pointing to a higher
361 concentration in contribution of glacial meltwater ($R^2=0.86$, $p<0.0001$). The absence of correlations for NO_x and PO_4 indicate
362 non-conservative mixing pointing towards the relevance of biological uptake and release ~~measurements~~-(Fig. 5d-f). At SG,
363 silicate concentrations were higher with lower salinities. The same pattern was observed in sea ice, ~~sealed to brine salinities,~~

364 with higher silicate and NO_x concentrations in the fresher SG ice, compared to NG and IE (Fig. 5g-i). However, the R² value
365 were lower in particular for Si(OH)₄ (NO_x: R²=0.18, p=0.059; Si(OH)₄: R²=0.41, p=0.002).

366 The contribution of nutrients by upwelling as well as freshwater inflow from glacial meltwater at SG was estimated by linear
367 mixing calculations for ~~the water layer~~ 1 m below the sea ice, avoiding the potential outlier values directly under the ice
368 (Eqs. Equations 1-6). At 1 m below the sea ice, about 32 ±0.1 % of the water was derived from glacial meltwater based on
369 salinity-based mixing of glacial meltwater and local Arctic water (Table 1, Eq. 1-2). The remaining 68 % came from either
370 bottom water upwelling (25 m at SG as reference) or ~~entrained~~-surface water (IE values at 1 m under the sea ice as reference).
371 Inorganic nutrients behaved conservatively at the IE reference (Fig. 5a-c), which allows similar mixing calculation of the
372 bottom water fraction. Based on ~~a similar estimation for inorganic~~ linear mixing of inorganic nutrients, 58 ±1 % of NO_x and
373 49 ±3 % of PO₄ was provided by subglacial upwelling (Table 1). For silicate, higher concentrations were required in the
374 bottom water of subglacial meltwater at the glacier front to explain the very high surface concentrations measured. Considering
375 the estimated NO_x and PO₄ fractions, the overall fraction of nutrients derived from upwelling was about 53 %. The overall
376 budget 1 m under the sea ice is was 32 ±0.1 % glacial meltwater, 53 ±3 % subglacial upwelling (marine bottom water), and
377 15 ±3 % horizontal transport (surface water).

378 3.3 Carbon cycle

379 Net primary productivity (NPP) was overall one order of magnitude higher at SG than at IE, with the highest production value
380 occurring within the brackish layer under the ice at SG (5.27 mg m⁻³ d⁻¹, Fig. 6, 7). Within this layer, also Chl values were
381 about two times higher compared to IE (21 mg m⁻³ at SG, 9.1 mg m⁻³ at IE), and also the Chl-specific productivity in this layer
382 exceeded values at the other stations (Table 2). Within sea ice, a slightly different pattern emerged. While the primary
383 productivity in the bottom sea ice (0–3 cm) was two times higher at SG compared to IE, Chl values were two order of
384 magnitudes lower (Fig. 6). This indicates high Chl-specific production at SG (5.6 mg C mg Chl d⁻¹ in the sea ice and 11.4 mg
385 C mg Chl d⁻¹ integrated over 25 m depth). At the IE, the contribution of released ice algae to algal biomass in the water column
386 was higher and the overall vertical Chl flux was about 1.5 times higher than at SG at 25 m depth. Bacterial biomass was
387 comparable at both stations with higher biomass concentrations within the ice than in the water column. Bacterial activity
388 (based on DCF) was comparable in the bottom sea ice at the two sites; however, it was 63x higher in the brackish surface water
389 of SG leading to very high growth rate estimates (Table 2) of 6 mg C m⁻³ d⁻¹. Due to a conversion factor from a very different
390 habitat (Molari et al., 2013), the absolute bacterial growth rate estimates are likely overestimations.

391 Integrated Chl values over the uppermost 25 m of the water column were nearly identical for SG and IE with values of about
392 3.75 mg Chl m⁻² (Table 2). The fraction of Chl was highest at IE (85 %) and lowest at the SG (30 %) (Table 2). The integrated
393 NPP was considerably higher at SG (42.6 mg C m⁻² d⁻¹ at SG, 0.2 mg C m⁻² d⁻¹ at IE), while the vertical export of Chl was
394 about three times higher at IE than SG. This leads to more (14 times) vertical export based on the sediment trap measurements
395 than production at IE and considerably lower (5 %) export than production at SG (Table 2). Relative to the standing stock
396 biomass of Chl at IE, 0.2 % of the Chl was renewed daily by NPP at IE and 3 % was vertically exported daily at IE, which

397 would relate - assuming absence of advection – to a daily loss of 3 % of the standing stock Chl. At SG, 38 % was renewed per
398 day, while 2 % were exported. As grazing was not estimated in this study, the suggested loss terms of Chl based on the sediment
399 trap data are likely underestimations. This leads to an accumulation of biomass of 38 % per day, and a doubling time of about
400 2.6 days. Bacterial growth doubling times were estimated to be between minutes (SG water) and days (IE water), but within
401 hours in sea ice (Table 2).

402 Considering the N demand based on the carbon based PP measurement (16 mol C mol N⁻¹ after Redfield, 1934), about 2 μmol
403 N L⁻¹ month⁻¹ (equivalent to 32 % of 1 m value for NO_x) was needed to sustain the PP measured at SG. Assuming constant PP
404 and steady state nutrient conditions, 32 % of the surface water had to be replaced by subglacial upwelling per month to supply
405 this N demand via upwelling. Since only 62 % of the upwelling water was entrained bottom water the actual vertical water
406 replenishment rate would be 52 % per month. Assuming a 2 m freshwater layer under the ice, this translates to flux of about
407 1.1 m³ m⁻² month⁻¹. Considering the distance of 250 m to the glacier front and a width of 1.6 km of the SG bay, this translates
408 to a minimum of about 422,000 m³ month⁻¹.

409 The reciprocal transplant experiment aimed to show the effect of water chemistry on primary production in the absence of
410 effects related to different communities, temperature, or light. The results (Fig. 7) showed clearly that the higher NPP at SG,
411 compared to NG was related to the ambient nutrient concentrations (nested ANOVA, p=0.0038, F=10.88). In any combination,
412 sterile filtered water from the SG had a fertilising effect on both SG and IE communities, increasing PP of IE communities by
413 approx. 30 %. SG communities of the most active fresh surface layer (4m1 m) fixed twice as much CO₂ when incubated in the
414 same water, compared to incubations in the IE water.

415 **3.4 Bacterial, archaeal and eukaryotic communities**

416 After bioinformatic processing 13,043 bacterial and archaeal (16S rRNA) OTUs, belonging to 1,208 genera with between
417 9,708 and 331,809 reads were retained. Differences between the bacterial 16S sequences of the various sample types indicated
418 that they can be used as potential markers for the origin of the water (Fig. 8). Sea ice and water communities were clearly
419 separated (ANOSIM, p=0.004, R=0.35) with no overlapping samples (Fig. 8a). Generally IE and NG communities were very
420 similar, while sea ice and under-ice water communities at SG were significantly different (ANOSIM, p=0.001, R=0.593) from
421 the other fjord samples. The NMDS showed also separation of 16S communities along a gradient from subglacial communities
422 towards fjord communities, with SG communities being in between fjord and subglacial communities (Fig. 8a). Bacterial
423 communities at SG in the bottom layer of the sea ice and the brackish water layer were more similar to subglacial outflow
424 communities than the other samples in both 2018 and 2019. Six OTUs were unique to the glacial outflow and SG surface
425 (closest relatives: *Fluviimonas*, *Corynebacterineae*, *Micrococcinae*, *Hymenobacter*, *Dolosigranum*), which are 6.6 % of their
426 OTUs. The community structure of supraglacial ice was very different from any other sample. Also in the most abundant
427 genera clear differences can be detected (Fig. S1). *Flavobacterium* sp. was most abundant in sea ice and UIW samples in both
428 2018 and 2019 at SG, but rare or absent in the other samples. *Aliiglaciecola* sp. was characteristic for NG sea ice and UIW
429 samples. *Paraglaciecola* sp. was abundant in NG and IE sea ice and UIW samples, and *Colwellia* sp. was abundant in all sea

430 ice and UIW samples. In ~~sea-water~~ seawater samples the genus *Amphritea* sp. was more abundant. *Pelagibacter* sp. was
431 abundant in all samples. Glacial outflow water was dominated by *Sphingomonas* sp. and glacier ice by *Halomonas* sp., which
432 were rare or absent in the other samples.

433 The eukaryotic community (18S rRNA) consisted of 4,711 OTUs, belonging to 535 genera, with between 2,204 and 15,862
434 reads. Overall, the same NMDS clustering has been found as for the 16S rRNA sequencing. We found distinctive communities
435 in the sea ice and 1 m layer under the sea ice at SG being significantly different (ANOSIM, $p=0.001$, $R=0.456$) to the other
436 samples (Fig. 8c). In fact, the SG surface communities were more similar to the outflow community (Fig. 8c). The clear
437 differentiation between all sea ice and water column communities was also visible in the 18S rRNA samples (ANOSIM,
438 $p=0.005$, $R=0.192$). As for the 16S communities, also the abundant genera differed between the groups (Fig. S2). The
439 cryptophytes *Hemiselmis* sp. and Geminigeraceae were abundant at SG, but rare at the other sites. Dinophyceae, Imbricatea
440 (*Thaumatomastix* sp.) and Bacillariophyceae were abundant in all samples with diatoms being mostly more abundant in sea
441 ice or UIW. The Chytridiomycota family of Lobulomycetaceae were abundant in water samples from 2018, but not 2019.
442 Subglacial outflow water was dominated by unclassified Cercozoa and *Bodomorpha* sp..

443 In total 22 different taxa were detected by microscopy. The community composition was clearly separated between sea ice and
444 water samples. Furthermore sea ice ~~algalspecies~~ composition at SG ~~station~~ differed from NG and IE (Fig. 8c). SG sea ice was
445 completely dominated by unidentified flagellates (potentially *Hemiselmis* sp., Geminigeraceae, and *Thaumatomastix* sp. based
446 on 18S sequences), with the exception of the 70–90 cm layer with high abundances of *Leptocylindrus minimus*. Sea ice samples
447 at NG and IE were dominated by the typical ~~Arctic~~-ice algae *Navicula* sp. and *Nitzschia frigida*. Water samples were more
448 diverse with high abundances of *Fragillariopsis* sp., *Coscinodiscus* sp., and *Chaetoceros* sp.. Overall, diatoms dominated most
449 samples at NG and IE in sea ice and water samples.

450 **4 Discussion**

451 The hydrography, sea ice properties, water chemistry and bacterial communities at SG provide clear evidence for submarine
452 discharge and upwelling at a shallow tidewater outlet glacier under sea ice, a system previously not considered for subglacial
453 upwelling processes. Briefly, our first hypothesis that submarine discharge persists also in early spring, supplying nutrient-
454 rich glacial meltwater and upwelling of bottom fjord water to the surface has been confirmed as discussed in detail below.

455 **4.1 Indications for submarine discharge and upwelling**

456 The physical properties at SG were distinctly different to stations NG and IE. In contrast to NG and IE, the marine terminating
457 SG site had a brackish surface water layer of 4 m thickness under the sea ice and low sea ice bulk salinities below ~~1.5-0.7~~ PSU,
458 with the exception of the uppermost 20 cm with a bulk salinity of 1.7 PSU. The sea ice bulk salinity is comparable to sea ice
459 in the nearby tidewater glacier influenced Tempelfjorden (Fransson et al., 2020) and ~~in~~-brackish Baltic sea ice (Granskog et
460 al., 2003). We excluded surface melt or river run-off as freshwater sources for the following reasons. With air temperatures

461 below freezing point during the sampling periods, surface runoff based on snowmelt was not possible and no melting was
462 observed during ~~field work~~fieldwork. In addition, ~~there were no~~major rivers are known to flow into the main bay
463 studied (Adolfbukta), ~~as indicated by~~due to the small catchment areas (Norsk Polarinstittut, 2020). We did observe some
464 subglacial runoff at the southern site of the glacier (close to SG), but this outflow water froze before it reached the fjord, which
465 was additionally blocked by a 1.33 m thick sea ice cover. The sea ice cover would also block any inputs by atmospheric
466 precipitation, considering the impermeable sea ice conditions especially at SG with brine volume fractions below 5 % (Golden
467 et al., 1998; Fransson et al., 2020). If surface runoff was present, we would also expect a similar pattern at the NG site. In fact,
468 due to the closer proximity to the southward facing mountains and higher sea ice permeability, NG would be more likely
469 influenced by surface runoff than SG. Additional~~Other~~ potential freshwater sources could be related to ~~terminus ice melt of~~
470 glacier fronts (Holmes et al., 2019; Sutherland et al., 2019), ~~or~~icebergs (Moon et al., 2018), or ice melange (Mortensen et al.,
471 2020). However, in the absence of Atlantic water inflow, which is blocked ~~in Billefjorden~~by a shallow sill depth at the entrance
472 of Billefjorden (Skogseth et al., 2020), water temperatures were consistently below the freezing point (max -0.2 °C) and no
473 Atlantic inflow water (Temperature ≥ 1 °C and Salinity ≥ 34.7 PSU, Skogseth et al., 2020) was detected at any station. These
474 low water temperatures do not allow glacier terminus ice to melt ~~in Billefjorden~~. Besides, Billefjorden is not characterized by
475 large amounts of icebergs or ice melange as described from Greenland glaciers (Moon et al., 2018; Mortensen et al., 2020).
476 However, glacier terminus ice melt is likely more important in systems with Atlantic water inflows, such as Greenland or
477 Svalbard fjords without a shallow sill (e.g. Kongsfjorden and Tunabreen, Holmes et al., 2019). Sea ice may melt at lower
478 temperatures compared to glacial ice, but the absence of typical sea ice algae in the water column at SG and the low salinity
479 of the sea ice indicated that this was not the case. In fact, sea ice with a salinity of 1.5 PSU (measured at SG) would melt at -
480 0.08 °C (Fofonoff et al., 1983), but the water and ice temperatures did not exceed -0.2 °C. In fact, at this temperature the
481 brackish surface water and meltwater of the submarine discharge would be supercooled. We did find a 1.5 cm layer of frazil
482 ice on the bottom of the SG sea ice showing that this did have some influence on sea ice formation. The subglacial meltwater
483 would need to introduce some heat, allowing the meltwater to reach the surface as liquid water. A temperature maximum at
484 the sea ice-water interface supports this hypothesis. This heat may also lead to basal sea ice melt as adding an~~additional~~ freshwater
485 source closer to the glacier front and main plume. However, sea ice melt as freshwater source cannot explain the low salinity
486 of the sea ice itself. Consistent with our study Fransson et al. (2020) also found substantial amount of freshwater in the sea ice
487 in Tempelfjorden (approx. 50 % meteoric water fraction) in a year with large glacier meltwater contribution further supporting
488 the presence of submarine discharge under sea ice in our study. Fransson et al. (2020) suggested the combination of low
489 salinities with ~~high~~high silicate concentrations as indicator for glacial meltwater contributions, which was also the case in our
490 study. In addition, the overall low sea ice ~~bulk~~ salinity and sediment inclusions at SG cannot be explained by sea ice melt, but
491 must originate from another source. Clear evidence for outflow comes also from the visual observations of subglacial outflow
492 exiting the land-terminating part south of the glacier in October 2019, April 2018 and April 2019, which we assume also
493 occurred under the marine terminating front. In fact, subglacial outflows in spring ~~have is a common phenomenon been~~
494 observed at various other Svalbard glaciers with runoff originating from meltwater stored under the glacier from the last melt

495 season and released by changes in hydrostatic pressure or glacier movements (Wadham et al., 2001). Active subglacial drainage
496 systems in winter have also been described elsewhere, and can be sustained by geothermal heat or frictional dissipation,
497 groundwater inputs, or temperate ice in the upper glacier (Wilson 2012; Schoof et al., 2014). This meltwater ~~can have~~ has also
498 been found to be rich in silicate ~~concentrations~~ due to the long contact with the subglacial bedrock during its storage over
499 winter (Wadham et al., 2001; Fransson et al., 2020). We therefore suggest that early spring submarine discharge is not unique
500 to Billefjorden, but likely occurs at all polythermal or warm based marine-terminating glaciers.

501 **4.2 Potential magnitude of submarine discharge and upwelling**

502 Considering the slow tidal currents in our study area (<22 m per 6 h tidal period, Kowalik et al., 2015) and wind mixing
503 blocked by sea ice, a potential source of the freshwater within Billefjorden may be meltwater introduced during the ~~last~~ late
504 summer to fall ~~melting~~ melt season and remaining throughout winter. Hence, the question of how much subglacial meltwater
505 reaches the surface ~~at SG~~ in what timeframe is important. We estimated that the ~~fresh~~ surface water was most likely exchanged
506 on time scales of days to weeks. Even slow vertical mixing would be capable to erode the halocline in over six months since
507 the last ~~melting~~ season. The turbidity peak that we observed at the halocline would also settle out in a short time (weeks), if
508 not replenished by fresh inputs (Meslard et al., 2018). ~~Vertical~~ We determined vertical export flux ~~was determined~~ to account
509 for approximately 4% of the Chl standing stock at 25 m- (Table 2). Considering that glacial sediment settles ~~typically~~
510 ~~substantially~~ typically much faster than phytoplankton due its higher density this suggests that the turbidity peak would erode
511 within days to weeks without fresh sediment inputs via upwelling (Meslard et al., 2018).

512 Furthermore, the inorganic nitrogen demand for the measured primary ~~productions~~ production would consume the present
513 nutrients in a few (approx. 2) months. Assuming steady state, the nutrient uptake by phytoplankton primary production would
514 require an upwelling driven water flux of at least $1.1 \text{ m}^3 \text{ m}^{-2} \text{ month}^{-1}$.

515 Microbial communities (16S rRNA and 18S rRNA) in SG UIW and sea ice were similar to the subglacial outflow water.
516 Bacterial communities (16S rRNA) at SG shared 6.6 % of their OTUs with subglacial outflow communities, which is twice as
517 much as NG and IE (3.6 %) shared with the outflow communities. Considering the estimated bacterial production and biomass
518 (Table 2) at SG the doubling time of the bacteria would be between 0.5 h and 7 h (Table 2). However, the use of a conversion
519 factor for biomass production based on sediment bacterial data is adding uncertainty to the estimation of the bacterial doubling
520 time. Estimates reported from Kongsfjorden in April are indeed longer (3-10 days, Iversen & Seuthe, 2010), as are other Arctic
521 bacterioplankton doubling time estimates ranging between 1.2 days (Rich et al., 1997), 2.8 days (de Kluijver et al., 2013) and
522 weeks (2 weeks, Rich et al., 1997; 1 week, Kirchman et al., 2005).

523 Based on the growth in the range of hours to days, the distinctive community at SG would have changed to a more marine
524 community on time scales of weeks, assuming only growth of marine OTUs at SG and settling out or grazing of inactive glacial
525 bacteria taxa. Thus, we suggest that the presence of shared OTUs between SG and the glacial outflow may indicate a continuous
526 supply of fresh inoculum to sustain these taxa. ~~Overall, our marine evidence based on salinity and nutrient profiles, turbidity,~~
527 ~~and communities support the occurrence of submarine discharge in early spring.~~

528 The amount of discharge and upwelling was estimated using hydrographic data. In our study, three water masses were
529 distinguished; i) subglacial outflow (SGO) with low salinity (0 PSU) relatively high temperatures (>0 °C) and high silicate
530 concentrations (Cape et al., 2019), (ii) deep local Arctic water (DLAW) entrained from approx. 20 m with low temperatures
531 (-1.7 °C) high salinities (34.76 PSU) and high nutrient concentrations (Skogseth et al., 2020), and iii) surface local Arctic water
532 (SLAW) with the same temperature and salinity signature as the DLAW, but depleted in nutrients (Skogseth et al., 2020).
533 Nutrients were depleted in the UIW, but not at 15 m depth, showing that the nutricline ~~had to be~~ shallower than 15 m.
534 Hence, submarine discharge ~~depth~~ at a glacier terminus depth of 20 m would be sufficient to cause upwelling of nutrient rich
535 DLAW to the surface. In fact, our mixing calculations (Equations 1-6) estimate that 32 % of the SG water 1 m under the sea
536 ice was derived by SGO, which pulled 1.6 times as much (53 % DLAW : 32 % SGO = ratio of 1.6) DLAW with it during
537 upwelling. Fransson et al. (2020) found that 30-60 % of glacier-derived meltwater was incorporated in the bottom sea ice at
538 the glacier front of Tempelfjorden, which is comparable to our study, again indicating that early spring submarine discharge
539 and the resulting formation of sea ice with low porosity is a widespread process at marine terminating glacier fronts in Svalbard.
540 Uncertainties with these estimates may be related to sea ice melt as additional freshwater source, and to slightly different
541 nutrient concentrations directly in the SG submarine discharge compared to the sampled subglacial outflow at some distance.

542 4.3 Importance of submarine discharge and upwelling under sea ice

543 To our knowledge, our study provides currently the only available estimate of subglacial upwelling in early spring. Our study
544 suggests that subglacial upwelling in spring causes results in Billefjorden a small volume transport of only about >1.1 m³ m⁻²
545 month⁻¹ (approx. 2 m³ s⁻¹) in Billefjorden. This estimate is based on the flux of nutrient rich bottom water needed to maintain
546 the measured primary production assuming steady state conditions and is therefore a rough, but conservative estimate. Due to
547 logistical limitations, we could not sample the submarine outflow directly at the SG site, but at some distance. Consequently,
548 submarine discharge at SG may have slightly different nutrient concentrations due to potentially different bedrock chemistry.
549 The most comparable estimate on the magnitude of the upwelling is available at Kronebreen for summer. This Svalbard
550 tidewater glacier is of similar size and had one ~~to two orders~~ of magnitude higher upwelling rates compared to our study
551 (31-127 m³ s⁻¹, Halbach et al., 2019). Due to their size, summer subglacial upwelling flux in Greenland is two to four times
552 higher than at Kronebreen (250-500 m³ s⁻¹, Carroll et al., 2016). In our study about 1.6 times as much bottom water from about
553 20 m (DLAW) as subglacial outflow water (SOW) reached the surface at SG (Entrainment factor of 1.6 – see above). The
554 entrainment factor is mostly dependent on the depth of the glacier front (Carroll et al., 2016). In fact, the glacier terminus at
555 SG was shallower (approx. 20 m) than any other studied tidewater glacier on Svalbard (70 m depth at Kronebreen, Halbach et
556 al., 2019) or Greenland (> 100 m, Hopwood et al., 2020), ~~explaining~~. Hence, the higher summer entrainment factors estimated
557 in Kongsfjorden (3, Halbach et al., 2019) and Greenland (6 to ~~1030~~, Hopwood et al., 2020) are not surprising. Glacier terminus
558 depth appears to be the main control of entrainment rates, likely independent of the time of the year. However, turbulent mixing
559 may cause increased entrainment during times of very high subglacial discharge rates. The higher entrainment factors in
560 Greenland also lead to more saline water reaching the surface and the strongly stratified brackish surface layer observed at SG

561 ~~has not been observed at these deep tidewater glaciers (e.g. Mortensen et al., 2020).~~ Kronebreen is the most comparable
562 tidewater glacier ~~to our study area~~ in terms of glacier terminus depth and entrainment rate. Although the estimated entrainment
563 factor was low at Kronebreen (3), ~~#submarine upwelling~~ substantially increased summer primary production in Kongsfjorden
564 (Halbach et al., 2019). ~~Despite~~In spite of the shallow depth, and the low discharge and entrainment rate of our study, subglacial
565 upwelling ~~was~~appears to be the main mechanism to replenish bottom water with high nutrient concentrations to the surface
566 and can substantially ~~increased~~increase spring primary production due to; (i) submarine outflow below (approx. 20 m) the
567 nutricline (<15 m), (ii) the absence of any other terrestrials inputs, (iii) Atlantic water blocked by a shallow sill (Skogseth et
568 al., 2020), (iv) very weak tidal currents (Kowalik et al., 2015), (iv) wind mixing blocked by sea ice in Billefjorden, and (v)
569 undiluted subglacial meltwater having lower nutrient concentrations than the DLAW.

570 **4.4 Importance for under-ice phytoplankton**

571 Our main finding was that i) higher irradiance, ii) a stratified surface layer, and iii) increased nutrient supply via subglacial
572 discharge and upwelling allowed increased phytoplankton primary production at SG. The ice edge station (IE) was light and
573 nutrient limited and supported a lower phytoplankton primary production.

574 **4.4.1 Increased light**

575 Despite the subglacial discharge and upwelling, the negative effect of light limitation with the massive sediment plumes in
576 summer (Pavlov et al., 2019) were not observed in early spring. We did measure a small turbidity peak under the SG sea ice,
577 but the values were comparable to open fjord systems in summer (Meslard et al., 2018, Pavlov et al., 2019), where light is
578 sufficient for photosynthesis. Under-ice phytoplankton blooms are typically limited by light, which is attenuated and reflected
579 by the snow and sea ice cover (Fortier et al., 2002, Mundy et al., 2009, Ardyna et al., 2020). Some blooms have been observed,
580 mostly under snow-free sea ice, such as after snow melt (Fortier et al., 2002), under melt ponds (Arrigo et al., 2012, Arrigo et
581 al., 2014), after rain events (Fortier et al., 2002), or at the ice edge related to wind-induced Ekman upwelling (Mundy et al.,
582 2009). In our study however, light levels available for phytoplankton growth were low compared to other under-ice
583 phytoplankton bloom studies (Mundy et al., 2009, Arrigo et al., 2012), but higher at SG than at IE. This can be explained
584 through the combined effects of sea ice and snow properties at SG. Light attenuation in low salinity sea ice is typically lower
585 due to a lower brine volume (Arst and Sipelgas, 2004). Also, lower sea ice algae biomass and thinner snow cover due to snow
586 removal with katabatic winds (e.g. Braaten 1997; Laska et al., 2012) leads to less light attenuation and a lower albedo. Our
587 estimates showed that about twice as much light reached the water at SG compared to the IE, in spite of the thicker sea ice
588 cover ~~and the~~. The estimated light levels of 5 and 9 $\mu\text{E m}^{-2} \text{s}^{-1}$ were above the minimum irradiance ($1 \mu\text{E m}^{-2} \text{s}^{-1}$) required for
589 primary production (Mock & Gradinger, 1999). Hence, the increased light under the brackish sea ice at SG could be one factor
590 explaining the under-ice phytoplankton bloom observed.

591 4.4.2 Stratified surface layer

592 The strong stratification at SG is another factor; allowing phytoplankton to stay close to the surface, where light is available,
593 allowing a bloom to form. In fact, Lowry et al. (2017) found that convective mixing by brine expulsion in refreezing leads can
594 inhibit phytoplankton blooms even in areas with sufficient under-ice light and nutrients. At the same time, they found moderate
595 phytoplankton blooms under snow covered sea ice (1–3 mg Chl m⁻³) sustained by a more stratified surface layer, which was,
596 however, still an order of magnitude lower than the SG values. Our finding of a higher vertical flux at IE compared to SG
597 shows that stronger stratification may indeed be a contributing factor for the higher phytoplankton biomass at SG due to lower
598 loss rate. However, our reciprocal transplant experiment clearly showed, that location alone (light, stratification) could not
599 explain the increased primary production, but that the water properties at SG had a fertilising effect on algal growth, most
600 probable because of higher nutrient levels, which were limiting at IE. In contrast to SG, higher plume entrainment factors at
601 deep Greenland tidewater glaciers (Hopwood et al., 2020), lead to subglacial meltwater typically highly diluted with saline
602 bottom water, once it reaches the surface, which leads to resulting in high salinities and a rather weak salinity driven
603 stratification directly at the glacier front (Mortensen et al., 2020). Hence, the strong effect on stratification may be a unique
604 feature of shallow tidewater glaciers.

605 4.4.3 Upwelling and meltwater influx of nutrients

606 Algal growth at IE was co-limited by lower irradiance as well as nutrient concentrations. Dissolved inorganic nitrogen (DIN)
607 to phosphate ratios (N:P) at the IE were mostly below Redfield ratios (16:1), especially in sea ice with DIN concentrations
608 below 1 µmol L⁻¹, indicating potential nitrogen limitations (Ptacnik et al., 2010), while the N:P ratio at SG was balanced and
609 close to Redfield. Silicate concentrations below 2 µmol L⁻¹ are typically considered limiting for diatom growth (Egge &
610 Aksnes, 1992) and this threshold had been reached at UIW and sea ice (concentration estimate in brine volume) at IE, but not
611 at SG. This indicates that nitrate supplied by bottom water upwelling and silicate by combined upwelling and additions from
612 the glacial ~~run-off~~runoff had a fertilising effect on the SG water. High silicate values have also been observed at glacier fronts
613 in other areas such as ~~the~~ Greenland fjords (Azetsu-Scott and Syvitski, 1997) and Tempelfjorden (Fransson et al., 2015:2020).
614 Iron has not been measured, but is an essential micronutrient, often enriched in subglacial meltwater (Bhatia et al., 2013,
615 Hopwood et al., 2020). However, iron limitation ~~typically does not occur~~is untypical in coastal Arctic systems (Krisch et al.,
616 2020). Besides the subglacial upwelling, nutrient concentrations ~~could~~may simply be higher due to ~~lower~~less physical forcing
617 and time needed for vertical mixing down to the bottom at the shallower water depth at SG compared to IE, ~~facilitating vertical~~
618 ~~mixing down to the bottom~~. However, NG was slightly shallower than SG and algal growth was still limited by nutrients.
619 Besides, silicate and nitrate showed negative correlations with salinity, when including SG samples. In fact, these nutrients
620 only correlated positively with salinity at IE and NG, while at SG, the negative correlations or non-conservative mixing are
621 indicative for subglacial upwelling (mainly N and Si) and/or meltwater input (for Si) (Hopwood et al., 2020). Biological
622 nutrient uptake did not play a significant role, due to relatively low bacterial and primary production. The subglacial outflow

623 water itself was poor in nitrate, but high in silicate due to the interaction with the subglacial bedrock and long residence time
624 below the glacier (Wadham et al., 2001), which was also found in ~~the~~ Tempelfjorden (Fransson et al., 2015; 2020).
625 Nordenskiöldbreen has a mix of metamorphic bedrock including silicon rich gneiss, amphibolite, and quartzite, but also
626 carbonate rich marble (Strzelecki, 2011), which can partly contribute to the high silicate levels observed. The role of bedrock
627 derived minerals and particles for composition of sea ice chemistry have been described in the neighbouring fjord
628 (Tempelfjorden) in detail by Fransson et al. (2020). Silicate concentrations in subglacial outflow water were lower ($<1.5 - 2$
629 $\mu\text{mol L}^{-1}$) compared to estimates in Greenland (Meire et al., 2016a, Hawkings et al., 2017, Hatton et al., 2019), indicating that
630 direct fertilisation in early spring may be even more important in other tidewater glacier influenced fjords. Another potential
631 source may be higher silicate concentrations in the sediments at SG (Hawkings et al., 2017). ~~However, While~~ bottom water
632 values were similar between SG and IE, ~~showing high concentrations in the SG sediments themselves is a limited role of higher~~
633 ~~silicate inputs from sediment, presumably due to silicate poor subglacial bedrock~~ probable source not accounted for in the
634 present study.
635 Another nitrogen source may be ammonium, which was introduced via subglacial upwelling in Kongsfjorden (Halbach et al.,
636 2019). Ammonium regeneration and subsequent nitrification (Christman et al., 2011) under the sea ice, may explain the
637 exceptionally high nitrate concentration of the UIW at SG, which can ~~partially explain~~ be part of the explanation for the high
638 N:P ratios. In fact, bacterial activity was higher at SG potentially allowing higher ammonium recycling. Another explanation
639 for the high N:P ratios and low phosphate concentrations ~~could~~ can be related to phosphate scavenging by iron, as discussed
640 by Cantoni et al. (2020). Nitrate can be supplied through the subglacial meltwater itself (Wynn et al., 2007), ~~however but~~
641 we did not find high nitrate concentrations in the undiluted subglacial outflow water in our study. Atmospheric inputs of N have
642 been shown in the Baltic Sea, but thinner sea ice and warm periods with increased sea ice permeability were needed for the N
643 to reach the brine pockets or water column (Granskog et al., 2003). Our NO_x profiles show some evidence of atmospheric N
644 deposition, but only at NG and SG, which may be related to precipitation or surface flooding. For under-ice phytoplankton,
645 these atmospheric N inputs play probably no role, but may have benefitted the high *Leptocylindrus* algae biomass layer in the
646 upper ice parts of SG. Overall, the clearest evidence of nutrient limitations and fertilisation by submarine discharge and
647 upwelling was demonstrated with the reciprocal transplant experiment, which showed an approx. 30 % increase in primary
648 production of algae communities incubated in SG water. Overall, primary production at SG was an order of magnitude higher
649 than at IE. This indicates that both fertilisation by submarine discharge and upwelling and increased light and stratification
650 play a role in increasing phytoplankton primary production.

651 **4.4.4 Increased phytoplankton primary production**

652 The integrated primary production to 25 m at SG was $42.6 \text{ mg C m}^{-2} \text{ d}^{-1}$ which is low compared to other marine terminating
653 glacier influenced fjord systems in summer with integrated NPP of $480 \pm 403 \text{ mg C m}^{-2} \text{ d}^{-1}$ (Hopwood et al., 2020), including
654 studies in Kongsfjorden on Svalbard with $250 - 900 \text{ mg C m}^{-2} \text{ d}^{-1}$ (Van de Poll et al., 2018). ~~A study~~ Also, studies conducted
655 ~~during a similar at the same~~ time window as ours (1 May) observed higher primary production rates in a marine-terminating

656 glacier influenced fjord system, ~~in~~such as Kongsfjorden (1520-1850 mg C m⁻² d⁻¹, Hodal et al., 2012). However, none of these
657 systems ~~was~~were sea ice covered during the ~~studies~~study periods and therefore not limited by light compared to our study.
658 Under sea ice, phytoplankton communities have typically much lower NPP rates of 20–310 mg C m⁻² d⁻¹ with only about 10
659 % or less light transmission reaching the water column (Mundy et al., 2009). These values are more comparable to the SG
660 values, despite the lower estimated light transmission (3 %). In the central Arctic, higher under-ice NPP has been
661 ~~observed~~measured, but always related to high light transmission due to the absence of ice, or under melt ponds with light
662 transmissions up to 59 % (Arrigo et al., 2012). However, in the sea ice area north of Svalbard, Assmy et al. (2017) found
663 substantial spring PP below relatively thick sea ice of refrozen leads. This was also confirmed by a large CO₂ decrease due to
664 primary production under the sea ice (Fransson et al., 2017). Phytoplankton production under snow covered Arctic sea ice is
665 often considered negligible compared to sea ice algae or summer production. This can be shown in low biomass, mostly
666 consisting of settling sea ice algae (Leu et al., 2015), or very low NPP rates (e.g. Pabi et al., 2008). The same has been observed
667 under Baltic sea ice with similar low light levels and primary production between 0.1–5 mg C m⁻² d⁻¹ under snow covered sea
668 ice and about 30 mg C m⁻² d⁻¹ under snow-free sea ice (Haecky & Andersson, 1999). These values are comparable to the IE
669 without subglacial meltwater influence, but an order of magnitude lower than the ~~SG~~-production at SG. Moderate blooms of
670 1–3 mg Chl m⁻³ have been described under snow covered sea ice with equal (3 %) light transmission (Lowry et al., 2017).
671 Lowry et al. (2017) argues that a stratified water column and sufficient nutrients allow moderate blooms even under these low
672 light conditions. In particular, diatoms, the most common taxa of under-ice phytoplankton blooms (von Quillfeldt, 2000, this
673 study) are known to be well adapted to low light conditions (Furnas, 1990). Our study found Chl values up to an order of
674 magnitude higher than Lowry et al. (2017), showing that under-ice phytoplankton blooms are indeed important under snow
675 covered sea ice and can be facilitated by submarine discharge and upwelling.

676 Our study is the first to show that the combination of several factors (stratified water column, increased light and supply of
677 fresh nutrients via tidewater glacier driven processes) can support a rather productive under-ice phytoplankton community,
678 exceeding biomass and production of under-ice phytoplankton in systems with comparable light levels. Besides the increased
679 and extended primary production ~~fuelled~~fuelled by tidewater glacier, the active and abundant phytoplankton taxa in surface
680 water with consistently replenished nutrients, may be a viable seed community for summer phytoplankton blooms, once the
681 sea ice disappears and light levels increase (Hegseth et al., 2019). The significantly different community at SG may also
682 contribute to an overall more diverse seed community available to the entire fjord, compared to fjords without early spring
683 subglacial discharge.

684 **4.5 Impact on sea ice algae**

685 **4.5.1 Impact on biomass and primary production**

686 While phytoplankton biomass and production were clearly ~~enhanced~~increased at SG, exceeding levels of other snow-covered
687 under-ice systems, sea ice algal biomass and activity had been differently affected. Our third hypothesis suggested lower sea

688 ice algae biomass and production at SG due to the lower brine volume fractions. In agreement with our hypothesis, algal
689 biomass was indeed an order of magnitude lower compared to the IE and NG. However, primary production was two times
690 higher, showing more efficient photosynthesis.

691 Compared to most other sea ice studies conducted ~~at~~during the same period of the year, typically representing the mid-bloom
692 phase with 10–20 mg Chl m⁻² (Leu et al., 2015), Chl biomass was very low at all stations of our study (<0.32 mg Chl m⁻²).
693 Only Greenland fjords (0.1–3.3 mg Chl m⁻²) or pre- and post-bloom systems had comparably low biomass (Mikkelsen et al.,
694 2008, Leu et al., 2015). The significantly different communities with a high number of cryptophyte flagellates, a high
695 proportion of phaeophytin (14–68 % in the bottom 3 cm), and a high contribution of sea ice algae in the water column indicate
696 that we sampled indeed a post-bloom situation. Considering the low air, sea ice and water temperatures and the absence of a
697 fresh UIW layer at the IE, the bloom was most likely not terminated by bottom ice erosion but ~~limited~~-by ~~nutrients~~-nutrient
698 ~~depletion~~. In fact, SG bottom ice was deficient in phosphate (0.27 μmol (L brine)⁻¹), while ~~the~~ IE was deficient in silicate (1
699 μmol (L brine)⁻¹) and nitrogen (N:P = 1 mol N mol P⁻¹). This finding fits to earlier studies where phosphate limitations had
700 been described as limiting for brackish sea ice algae at concentrations below 0.27 μmol L⁻¹ (Haecky and Andersson, 1999),
701 while N and Si limitations are typical for Arctic sea ice algae (Gradinger, 2009). The low concentrations of phosphate in the
702 subglacial meltwater would partly explain the low concentration in SG sea ice. In addition, most studies summarized by Leu
703 et al. (2015) were done 10 years or more prior to our measurements. In fact, the Greenland study by Mikkelsen et al. (2008)
704 with comparable sea ice algae biomass had the thinnest sea ice cover of 0.5 m sampled in the warmest year (2006). During our
705 study, the weather station in Longyearbyen measured a mean temperature of –3.9 °C in April 2019, which was 8.3 °C above
706 average and the second warmest average April temperature recorded after April 2006 (0.1 °C), indicating that a warmer climate
707 may explain the earlier bloom termination (yr.no).

708 Similar to algal biomass, primary production (approx. 0.01 mg C m⁻² d⁻¹ at SG and 0.005 mg C m⁻² d⁻¹ at IE, assuming 10 cm
709 productive bottom layer) was considerably lower than in most studies of Arctic sea ice (0.8–55 mg C m⁻² d⁻¹ in the Barents
710 Sea) mentioned by Leu et al.(2015). Only studies on algal aggregates (Assmy et al., 2013) and Baltic sea ice (Haecky &
711 Andersson, 1999) measured similarly low production rates indicating that the senescence of the bloom (aggregates) and brine
712 volume fraction (Baltic Sea) were factors contributing to low primary production in sea ice.

713 4.5.2 Stressors in brackish sea ice

714 In addition to the post bloom status of the bloom, the lower biomass at SG can be partly explained by the lower brine salinity.
715 Permeability of sea ice is typically related to salinity and temperature, which determine the brine volume. With a brine volume
716 fraction below 5 %, or a temperature below -5 °C and a salinity below 5 PSU, sea ice is considered impermeable (Golden et
717 al., 1998). At SG, temperatures were higher, but a brine volume fraction above 5 % was only found in bottom ice sections (7–
718 9 %), indicating that the brine channels are weakly connected and algae had limited inhabitable place and nutrient supply
719 (Granskog et al., 2003), especially in the upper layers of the sea ice. In more saline systems, such as the ~~Chuekehi~~Chukchi or
720 Beaufort Sea a high flux of seawater through the ice (0.4–19 m³ seawater m⁻² sea ice) has been discussed as crucial to allow

721 continuous primary production and accumulation of biomass (Gradinger, 2009). In impermeable ice, this flux is eliminated.
722 However, the algal biomass at SG was very low, even compared to other brackish sea ice system, such as the Baltic Sea with
723 similar or lower brine volume fractions and comparable light levels (Granskog et al., 2003: 3-6 mg Chl m⁻³; Haecky &
724 Andersson, 1999: 1.2 mg Chl m⁻²), indicating that other stressors played a role at SG. Grazing is assumed to be a minor control
725 on algae production and biomass in Arctic sea ice (Gradinger, 2002). However, grazing by heterotrophic flagellates on small
726 primary producers has been described as important in the Baltic Sea, indicating that it might ~~playsplay~~ a role at SG as well
727 (Haecky & Andersson, 1999). SG sea ice communities were indeed dominated by small flagellate algae (microscopy based)
728 and a high proportion of potential grazers (18S rRNA data). Other stressors, such as phosphate limitation, viral lysis, or osmotic
729 stress related to episodic outbursts of subglacial meltwater are likely additional factors explaining the low biomass.
730 DIC has also been described as potentially limiting for sea ice primary production, especially towards the end of the bloom
731 (Haecky & Andersson, 1999) and may be supplied with the carbonate rich subglacial outflow (Fransson et al., 2020). Higher
732 mortality due to factors mentioned above, together with the higher measured bacterial activity, allowing recycling of nutrients
733 may be ~~anothera~~ factor explaining higher production with lower Chl biomass. ~~Last~~Lastly, nutrients may have been replenished
734 recently via advective processes when the brine volume fraction was higher.
735 At SG, another layer of potentially high activity has been found in the upper sea ice. In this layer, depleted nutrient
736 concentrations ~~correspond~~corresponded with high *Leptocylindrus minimus* abundances indicating that these algae were
737 actively taking up the nutrients, despite the impermeable sea ice. NO_x concentrations increased towards the surface and bottom
738 indicating inputs from surface flooding above (Granskog et al., 2003) and seawater below. Silicate and phosphate were only
739 supplied from the seawater below. The observed brine volume fractions below 5 % would not allow inputs of these nutrients,
740 but episodes with higher temperatures and thereby higher brine volume fractions may be sufficient to supply the needed
741 nutrients to this distinctive layer.
742 Overall, sea ice influenced by subglacial outflow was very similar to other brackish sea ice such as in the Baltic Sea ~~in regard~~
743 ~~to~~concerning structure, biomass and production (Haecky & Andersson, 1999, Granskog et al., 2005). Compared to Arctic sea
744 ice ~~the effect was negative on~~ sea ice algae biomass was reduced due to low brine volume fractions, phosphate limitation and
745 potentially higher mortality via grazing and possibly higher osmotic stress.

746 **5 Outlook**

747 Our study showed that even a shallow marine-terminating glacier can lead to increased under-ice phytoplankton production
748 by locally enhanced light levels, stronger stratification and nutrient supply by submarine discharge and upwelling, which are
749 all factors expected to change due to climate change. While ~~most~~much of our evidence is circumstantial, the number of different
750 lines of evidence leading to the same conclusion makes our findings rather robust. We propose that our findings are applicable
751 to other shallow tidewater glaciers with a polythermal or warm base, as is common on Svalbard, ~~but also on Greenland~~ (Hagen
752 et al., 1993; Irvine-Fynn et al., 2011). In the shorter term, a longer melt season and presumably increased submarine discharge
753 may lead to increased subglacial upwelling in winter and spring. However, on longer time scales, glaciers will retreat and

754 transform towards land terminating glaciers (Błaszczuk et al., 2009), which would result in the lack of submarine discharge
755 and systems more similar to the NG and IE with less nutrients and light available for phytoplankton. The local effect would
756 reduce primary production, biomass and bacterial production in the water column, but would result in higher biomass of sea
757 ice algae with the known Arctic taxa of pennate diatoms. TheConsidering the increased sedimentation rate at IE, we expect
758 the pelagic/sympagic benthic coupling would-beto become stronger supporting the benthic food web. Winter and spring
759 submarine discharge is most likely present at all polythermal or warm-based marine-terminating glaciers, which includes
760 glacier terminatermini with much deeper fronts, much higher entrainment rates of bottom water, and higher silicate
761 concentrations in the glacial meltwater (Hopwood et al., 2020). Thus, the effect of early spring submarine discharge is likely
762 more pronounced in other fjords. Additional effects of climate change include increased precipitation in the Arctic, which
763 would reduce light levels below the sea ice. However, also land-terminating glaciers would allow snow removal by katabatic
764 wind as discussed for Nordenskiöldbreen.

765 Another impact of climate change will be the reduction and earlier break-up of sea ice and Atlantification of fjords, leading to
766 increased light, and wind mixing. In the ice free Kongsfjorden, higher primary production rates have been measured in the
767 same month, indicating that the lack of sea ice may lead to increased overall primary production (Iversen & Seuthe, 2010).
768 However, Kongsfjorden is still influenced by subglacial upwelling, supplying nutrients for the bloom (Halbach et al., 2017).
769 In systems not affected by subglacial upwelling the additional light will most likely not lead to substantially higher primary
770 production as indicated by lower measured rates in these type of fjords (Hopwood et al., 2020). Since the entrainment in our
771 study occurs at only approximately 20 m depth, upwelling under sea ice-free conditions would have much less effect, since
772 wind induced vertical-mixing plays a more important role. Direct silicate fertilisation would also have less effect in an ice-free
773 fjord since the fjord phytoplankton biomass is likely more nitrate than silicate limited, due to the later stage of the spring bloom
774 (Hegseth et al., 2019). In summary, we suggest that subglacial upwelling in early spring is important for phytoplankton blooms,
775 but only in a sea-ice covered fjord. The future of the spring phytoplankton blooms depends on what happens first,
776 disappearance of sea ice, or retreat of the glacier to land.

777 **6 Acknowledgements**

778 The field was funded by the individual Arctic field grants of the Svalbard Science forum for TV, UD, CD, and EH (project
779 numbers: 282622 (TV, UD, CD), 282600 (TV), 296538 (EH), 281806 (UD)). Additional, funding for lab work and analyses
780 was obtained by the ArcticSIZE - A research group on the productive Marginal Ice Zone at UiT (grant no. 01vm/h15). JE was
781 also supported by the the Ministry of Education, Youth and Sports of the Czech Republic ECOPOLARIS, project No.
782 CZ.02.1.01/0.0/0.0/16_013/0001708 and the Institute of Botany CAS (grant no. RVO 67985939). The publication charges for
783 this article have been partly funded by a grant from the publication fund of UiT The Arctic University of Norway.

784 We also wish to thank Jan Pechar, Jiří Štojd, and Marie Šabacká for field assistance; and Janne Søreide, Maja Hatlebekk,
785 Christian Zoelly, Marek Brož, Stuart Thomson, and Tore Haukås for field work preparation help. We are also acknowledged

786 to Melissa Brandner, Paul Dubourg, and Claire Mourgues for the help in the lab and Owen Wangensteen for the help with
787 bioinformatics analyses. We are thankful for the meteorological data of Petuniabukta supplied by Kamil Laska.

788 **7 Authors contributions**

789 TRV designed the experiments, formulated the hypotheses and developed the sampling design with contributions of CD and
790 UD, and RG. Fieldwork was conducted by TRV, UD, CD, EH, and JE with support by RG and EP for preparations. Lab
791 analyses were done by TRV, UD, EP, CD, MC and EH. Computational analyses were performed by TRV. The manuscript has
792 been prepared by TRV with contributions of all co-authors.

793 **8 Data availability**

794 Environmental data have been archived at Dataverse under the doi number <https://doi.org/10.18710/MTPR9E>. 18S and 16S
795 rRNA sequences have been archived at the European Nucleotide archive under the project accession number PRJEB40294.
796 The R and unix code for the statistical and bioinformatics analyses are available from the corresponding author upon request.
797 More detailed reports of the fieldwork are available in the Research in Svalbard database under the RiS-ID 10889.

798 **9 Competing interests**

799 The authors declare that they have no conflict of interest.

800 **References**

- 801 Ambrožová, K., and Láska, K.: Air temperature variability in the vertical profile over the coastal area of Petuniabukta, central
802 Spitsbergen, Polish Polar Research, 41-60, 2017.
- 803 Amundson, J. M., and Carroll, D.: Effect of topography on subglacial discharge and submarine melting during tidewater glacier
804 retreat, Journal of Geophysical Research: Earth Surface, 123(1), 66-79, 2018.
- 805 Ardyna, M., Mundy, C. J., Mills, M. M., Oziel, L., Grondin, P. L., Lacour, L., Verin, G., Van Dijken, G., Ras, J., Alou-Font,
806 E., Babin, M., Gosselin, M., Tremblay, J. É., Raimbault, P., Assmy, P., Nicolaus, M., Claustre, H. and Arrigo, K.R.:
807 Environmental drivers of under-ice phytoplankton bloom dynamics in the Arctic Ocean, Elem Sci Anth, 8(1), 30, DOI:
808 <http://doi.org/10.1525/elementa.430>,<http://doi.org/10.1525/elementa.430>, 2020.
- 809 Arrigo, K. R., Perovich, D. K., Pickart, R. S., Brown, Z. W., vanDijken, G. L., Lowry, K. E., Mills, M. M., Palmer, M. A.,
810 Balch, W. M., Bahr, F., Bates, N. R., Benitez-Nelson, C., Bowler, B., Brownlee, E., Ehn, J. K., Frey, K. E., Garley, R.,
811 Laney, S.R., Lubelczyk, L., Mathis, J., Matsuoka, A., Mitchell, G. B., Moore, G. W. K., Ortega-Retuerta, E., Pal, S.,

812 Polashenski, C.M., Reynolds, R. A., Schieber, B., Sosik, H. M., Stephens, M.,P., and Swift, J. H.: Massive phytoplankton
813 blooms under Arctic sea ice, *Science*, 336, 1408, <https://org/10.1126/science.1215065>, 2012.

814 Arrigo, K. R., Arrigo, K. R., Perovich, D. K., Pickart, R. S., Brown, Z. W., van Dijken, G. L., Lowry, K. E., Mills, M. M.,
815 Palmer, M. A., Balch, W. M., Bates, N. R., Benitez-Nelson, C. R., Brownlee, E., Frey, K. E., Laney, S. R., Mathis, J., Matsuoka,
816 A., Mitchell, B. G., Moore, G. W. K., Reynolds, R. A., Sosik, H. A., Swift, J. H.: Phytoplankton blooms beneath the sea ice in
817 the Chukchi Sea, *Deep Sea Res. Part II Top. Stud. Oceanogr.*, 105, 1-16, <https://org/10.1016/j.dsr2.2014.03.018>, 2014.

818 Arst, H., and Sipelgas, L.: In situ and satellite investigations of optical properties of the ice cover in the Baltic Sea region, in:
819 *Proceedings of the Estonian Academy of Sciences, Biology and Ecology*, edited by: Aben, H., and Kurnitski, V., Estonian
820 Academy of Sciences, Tallinn, 25-36, 2004.

821 Assmy, P., Ehn, J. K., Fernández-Méndez, M., Hop, H., Katlein, C., Sundfjord, A., Bluhm, K., Daaase, M., Engel, A., Fransson,
822 A., Granskog, M. A., Hudson, S. R., Kristiansen, S., Nicolaus, M., Peeken, I., Renner, A. H. H., Spreen, G., Tatarek, A., and
823 Wiktor, J.: Floating ice-algal aggregates below melting Arctic sea ice, *PLoS ONE*, 8(10), e76599,
824 <https://org/10.1371/journal.pone.0076599>, 2013.

825 Assmy, P., M. Fernández-Méndez, P. Duarte, A. Meyer, A. Randelhoff, C. J. Mundy, L. M. Olsen, H. M. Kauko, A. Bailey, and
826 Chierici, M.: Leads in Arctic pack ice enable early phytoplankton blooms below snow-covered sea ice, *Scientific reports*, 7,
827 40850, 2017.

828 Atienza, S., Guardiola, M., Präbel, K., Antich, A., Turon, X., and Wangensteen, O. S.: DNA Metabarcoding of Deep-Sea
829 Sediment Communities Using COI: Community Assessment, Spatio-Temporal Patterns and Comparison with 18S rDNA,
830 *Diversity*, 12(4), 123, <https://org/10.3390/d12040123>, 2020.

831 Azetsu-Scott, K., and Syvitski, J. P. M.: Influence of melting icebergs on distribution, characteristics and transport of marine
832 particles in an East Greenland fjord, *Journal of Geophysical Research* 104 (C3), 5321–5328, 1999.

833 Bhatia, M. P., Kujawinski, E. B., Das, S. B., Breier, C. F., Henderson, P. B., and Charette, M. A.: Greenland meltwater as a
834 significant and potentially bioavailable source of iron to the ocean, *Nat Geosci*, 6(4), 274-278, <https://org/10.1038/ngeo1746>,
835 2013.

836 Błaszczyk, M., Jania, J. A., and Hagen, J. O.: Tidewater glaciers of Svalbard: Recent changes and estimates of calving fluxes,
837 *Pol Polar Res*, 2, 85-142, 2009.

838 Boyer, F., Mercier, C., Bonin, A., Le Bras, Y., Taberlet, P., and Coissac, E.: obitools: A unix-inspired software package for
839 DNA metabarcoding, *Mol Ecol Resour*, 16(1), 176-182, <https://org/10.1111/1755-0998.12428>, 2016.

840 Braaten, D. A.: A detailed assessment of snow accumulation in katabatic wind areas on the Ross Ice Shelf, Antarctica, *J*
841 *Geophys Res Atmos*, 102(D25), 30047-30058, <https://org/10.1029/97JD02337>, 1997.

842 Cantoni, C., Hopwood, M. J., Clarke, J. S., Chiggiato, J., Achterberg, E. P., and Cozzi, S.: Glacial drivers of marine
843 biogeochemistry indicate a future shift to more corrosive conditions in an Arctic fjord, *Journal of Geophysical Research:*
844 *Biogeosciences*, e2020JG005633,
845 <https://doi.org/https://doi.org/10.1029/2020JG005633>, <https://doi.org/https://doi.org/10.1029/2020JG005633>, 2020.

846 Carroll, D., Sutherland, D. A., Hudson, B., Moon, T., Catania, G. A., Shroyer, E. L., Nash, J. D., Bartholomew, T. C., Felikson,
847 D., Stearns, L. A., Noël, B. P. Y., and van den Broeke, M. R.: The impact of glacier geometry on meltwater plume structure
848 and submarine melt in Greenland fjords, *Geophys. Res. Lett.*, 43, 9739–9748, <https://doi.org/10.1002/2016GL070170>, 2016.

849 Chandler, D. M., Wadhwa, J. L., Lis, G. P., Cowton, T., Sole, A., Bartholomew, I., Telling, J., Nienow, P., Bagshaw, E.B.,
850 Mair, D., Vinen, S., and Hubbard A.: Evolution of the subglacial drainage system beneath the Greenland Ice Sheet revealed
851 by tracers, *Nat Geosci.*, 6(3), 195-198, <https://org/10.1038/ngeo1737>, 2013.

852 Christman, G. D., Cottrell, M. T., Popp, B. N., Gier, E., and Kirchman, D. L.: Abundance, diversity, and activity of ammonia-
853 oxidizing prokaryotes in the coastal Arctic Ocean in summer and winter, *Appl. Environ. Microbiol.*, 77(6), 2026-2034,
854 <https://org/10.1128/AEM.01907-10>, 2011

855 Cloern, J. E., Grenz, C., and Videgar-Lucas, L.: An empirical model of the phytoplankton chlorophyll: carbon ratio-the
856 conversion factor between productivity and growth rate, *Limnol. Oceanogr.*, 40(7), 1313-1321,
857 <https://org/10.4319/lo.1995.40.7.1313>, 1995.

858 Cox, G. F., and Weeks, W. F.: Equations for determining the gas and brine volumes in sea-ice samples, *J Glaciol.*, 29(102),
859 306-316, <https://org/10.3189/S0022143000008364>, 1983.

860 De Kluijver, A., Soetaert, K., Czerny, J., Schulz, K. G., Boxhammer, T., Riebesell, U., and Middelburg, J. J.: A ¹³C labelling
861 study on carbon fluxes in Arctic plankton communities under elevated CO₂ levels, *Biogeosciences*, 10(3), 1425-1440, 2013.

862 Dickson, A. G., Sabine, C. L., and Christian, J. R.: Guide to best practices for ocean CO₂ measurements, PICES Special
863 Publication 3, 2007.

864 Dowdeswell, J. A.: On the nature of Svalbard icebergs, *J Glaciol.*, 35(120), 224-234, <https://org/10.3189/S002214300000455X>,
865 1989.

866 Egge, J. K., and Aksnes, D.L.: Silicate as regulating nutrient in phytoplankton competition, *Mar Ecol Prog ser.* Oldendorf, 83,
867 281-289, <https://org/10.3354/meps083281>, 1992.

868 Esau, I., and Repina, I.: Wind climate in Kongsfjorden, Svalbard, and attribution of leading wind driving mechanisms through
869 turbulence-resolving simulations, *Advances in Meteorology*, <https://org/10.1155/2012/568454>, 2012.

870 Fransson, A., Chierci, M., Nomura, D., Granskog, M. A., Kristiansen, S., Martma, T., and Nehrke, G.: Influence of glacialwater
871 and carbonate minerals on wintertime sea-ice biogeochemistry and the CO₂ system in an Arctic fjord in Svalbard, *Annals of*
872 *Glaciology*, 1–21, <https://doi.org/10.1017/aog.2020.52>; <https://doi.org/10.1017/aog.2020.52>, 2020.

873 Fransson, A., Chierici, M., Skjelvan, I., Olsen, A., Assmy, P., Peterson, A., Spreen, G., and Ward, B.: Effect of sea-ice and
874 biogeochemical processes and storms on under-ice water fCO₂ during the winter-spring transition in the high Arctic Ocean:
875 implications for sea-air CO₂ fluxes, *J. Geophys. Res. Oceans*, 122, 5566–5587, doi: 10.1002/2016JC012478, 2017.

876 Fofonoff, P., and Millard R. C.: Algorithms for computation of fundamental properties of seawater, *Unesco Technical Papers*
877 *in Marine Science*, 44, 53, <http://hdl.handle.net/11329/109>, 1983.

878 Fortier, M., Fortier, L., Michel, C., and Legendre, L.: Climatic and biological forcing of the vertical flux of biogenic particles
879 under seasonal Arctic sea ice, *Mar. Ecol. Prog. Ser.*, 225, 1-16, <https://org/10.3354/meps225001>, 2002.

880 Furnas, M. J.: In situ growth rates of marine phytoplankton: approaches to measurement, community and species growth rate,
881 *J Plankton Res*, 12, 1117–1151, 1990.

882 Garrison, D. L., and Buck, K. R.: Organism losses during ice melting: a serious bias in sea ice community studies, *Polar Biol*
883 6:237-239, 1986.

884 Golden, K. M., Ackley, S. F., and Lytle, V. I.: The percolation phase transition in sea ice, *Science*, 282(5397), 2238-2241,
885 <https://org/10.1126/science.282.5397.2238>, 1998.

886 Gradinger, R.: Sea ice microorganisms, *Encyclopedia of environmental microbiology*, Wiley,
887 <https://org/10.1002/0471263397.env310>, 2003.

888 Gradinger, R.: Sea-ice algae: Major contributors to primary production and algal biomass in the Chukchi and Beaufort Seas
889 during May/June 2002, *Deep Sea Res. Part II Top. Stud. Oceanogr.*, 56(17), 1201-1212,
890 <https://org/10.1016/j.dsr2.2008.10.016>, 2009.

891 Granskog, M. A., Kaartokallio, H., and Shirasawa, K.: Nutrient status of Baltic Sea ice: Evidence for control by snow-ice
892 formation, ice permeability, and ice algae, *J Geophys Res Oceans*, 108(C8), <https://org/10.1029/2002JC001386>, 2003.

893 Guardiola, M., Uriz, M. J., Taberlet, P., Coissac, E., Wangensteen, O. S., and Turon, X.: Deep-sea, deep-sequencing:
894 metabarcoding extracellular DNA from sediments of marine canyons, *PloS one*, 10(10), e0139633, 2015.

895 Haecky, P., and Andersson, A.: Primary and bacterial production in sea ice in the northern Baltic Sea, *Aquat Microb Ecol*,
896 20(2), 107-118, <https://org/10.3354/ame020107>, 1999.

897 Hagen, J. O., Liestøl, O., Roland, E., and Jørgensen, T.: *Glacier Atlas of Svalbard and Jan Mayen*, Oslo: Norwegian Polar
898 Institute, 1993.

899 Halbach, L., Vihtakari, M., Duarte, P., Everett, A., Granskog, M. A., Hop, H., Kauko, H. M., Kristiansen, S., Myhre, P. I.,
900 Pavlov, A. K., Pramanik, A., Tatarek, A., Torsvik, T., Wiktor, J. M., Wold, A., Wulff, A., Steen, H., Assmy, P.: Tidewater
901 glaciers and bedrock characteristics control the phytoplankton growth environment in a fjord in the arctic, *Front Mar Sci*, 6,
902 254, <https://org/10.3389/fmars.2019.00254>, 2019.

903 Hatton, J. E., Hendry, K. R., Hawkings, J. R., Wadham, J. L., Kohler, T. J., Stibal, M., Beaton, A. D., Bagshaw, E. A., and
904 Telling, J.: Investigation of subglacial weathering under the Greenland Ice Sheet using silicon isotopes, *Geochim Cosmochim*
905 *Acta*, 247, 191-206, <https://org/10.1016/j.gca.2018.12.033>, 2019.

906 Hawkings, J. R., Wadham, J. L., Benning, L. G., Hendry, K. R., Tranter, M., Tedstone, A., Nienow, P., and Raiswell, R.: Ice
907 sheets as a missing source of silica to the polar oceans, *Nat. Commun*, 8(1), 1-10, <https://org/10.1038/ncomms14198>, 2017.

908 Hegseth, E. N., Assmy, P., Wiktor, J. M., Wiktor, J., Kristiansen, S., Leu, E., Tverberg, V., Gabrielsen, T. M., Skogseth, R.,
909 and Cottier, F.: Phytoplankton seasonal dynamics in Kongsfjorden, Svalbard and the adjacent shelf, in: *The Ecosystem of*
910 *Kongsfjorden, Svalbard*, edited by: Hop, H., and Wiencke, C., Springer, Cham., 173-227, 2019.

911 Hodal, H., Falk-Petersen, S., Hop, H., Kristiansen, S., and Reigstad, M.: Spring bloom dynamics in Kongsfjorden, Svalbard:
912 nutrients, phytoplankton, protozoans and primary production, *Polar Biol* 35, 191–203, [https://doi.org/10.1007/s00300-011-](https://doi.org/10.1007/s00300-011-1053-7)
913 [1053-7](https://doi.org/10.1007/s00300-011-1053-7), <https://doi.org/10.1007/s00300-011-1053-7>, 2012.

914 Hodgkins, R.: Glacier hydrology in Svalbard, Norwegian high arctic, *Quat Sci Rev*, 16(9), 957-973, <https://org/10.1016/S0277->
915 3791(97)00032-2, 1997.

916 Holmes, F. A., Kirchner, N., Kuttenukeuler, J., Krützfeldt, J., and Noormets, R.: Relating ocean temperatures to frontal ablation
917 rates at Svalbard tidewater glaciers: Insights from glacier proximal datasets, *Sci. Rep.*, 9(1), 1-11, <https://org/10.1038/s41598->
918 019-45077-3, 2019.

919 Hopwood, M. J., Carroll, D., Dunse, T., Hodson, A., Holding, J. M., Iriarte, J. L., Ribeiro, S., Achterberg, E. P., Cantoni, C.,
920 Carlson, D. F., Chierici, M., Clarke, J. S., Cozzi, S., Fransson, A., Juul-Pedersen, T., Winding, M. S. and Meire, L.: How does
921 glacier discharge affect marine biogeochemistry and primary production in the Arctic?, *Cryosphere*, 14, 1347-1383, <https://org/>
922 10.5194/tc-14-1347-2020, 2020.

923 Irvine-Fynn, T. D., Hodson, A. J., Moorman, B. J., Vatne, G., & Hubbard, A. L.: Polythermal glacier hydrology: A review,
924 *Reviews of Geophysics*, 49(4), 2011.

925 Iversen, K. R., and Seuthe, L.: Seasonal microbial processes in a high-latitude fjord (Kongsfjorden, Svalbard): I. Heterotrophic
926 bacteria, picoplankton and nanoflagellates, *Polar Biol*, 34(5), 731-749, <https://org/10.1007/s00300-010-0929-2>, 2011.

927 Jones, E., Chierici, M., Skjelvan, I., Norli, M., Børsheim, K. Y., Lødemel, H. H., Sørensen, K., King, A. L., Lauvset, S.,
928 Jackson, K., de Lange, T., Johannessen, T., and Mourgues, C.: Monitoring ocean acidification in Norwegian seas in 2018,
929 *Miljødirektoratet*, M-1417/2019, 2019.

930 Kanna, N., Sugiyama, S., Ohashi, Y., Sakakibara, D., Fukamachi, Y., and Nomura, D.: Upwelling of macronutrients and
931 dissolved inorganic carbon by a subglacial freshwater driven plume in Bowdoin Fjord, northwestern Greenland, *J Geophys*
932 *Res Biogeosci*, 123(5), 1666-1682, <https://org/10.1029/2017JG004248>, 2018.

933 Kartverket, <https://kartkatalog.geonorge.no/metadata/kartverket/dybdedata/2751aacf-5472-4850-a208-3532a51c529a>, last
934 access: 10 August 2020.

935 Kirchman, D. L., Malmstrom, R. R., and Cottrell, M. T.: Control of bacterial growth by temperature and organic matter in the
936 Western Arctic, *Deep Sea Research Part II: Topical Studies in Oceanography*, 52(24-26), 3386-3395, 2005.

937 Kowalik, Z., Marchenko, A., Brazhnikov, D., and Marchenko, N.: Tidal currents in the western Svalbard Fjords, *Oceanologia*,
938 57(4), 318-327, <https://org/10.1016/j.oceano.2015.06.003>, 2015.

939 Krisch, S., Browning, T. J., Graeve, M., Ludwichowski, K.U., Lodeiro, P., Hopwood, M. J., Roig, S., Yong, J. C., Kanzow,
940 T., and Achterberg, E. P.: The Influence of Arctic Fe and Atlantic Fixed N on Summertime Primary Production in Fram Strait,
941 North Greenland Sea, *Sci. Rep.*, 10 (1), 15230, <https://doi.org/10.1038/s41598-020-72100-9>, 2020.

942 Leppäranta, M., and Manninen, T.: The brine and gas content of sea ice with attention to low salinities and high temperatures,
943 *Finnish Institute of Marine Research Internal Report*, 2, 1-15, 1988.

944 Láska, K., Witoszová, D., and Prošek, P.: Weather patterns of the coastal zone of Petuniabukta, central Spitsbergen in the
945 period 2008–2010, *Polish Polar Research*, 297-318, 2012.

946 Leu, E., Mundy, C. J., Assmy, P., Campbell, K., Gabrielsen, T. M., Gosselin, M., Juul-Pedersen, T., and Gradinger, R.: Arctic
947 spring awakening—Steering principles behind the phenology of vernal ice algal blooms, *Prog Oceanogr*, 139, 151-170,
948 <https://org/10.1016/j.pocean.2015.07.012>, 2015.

949 Lowry, K. E., Pickart, R. S., Selz, V., Mills, M. M., Pacini, A., Lewis, K. M., Joy-Warren, H., Nobre, C., van Dijken, G. L.,
950 Grondin, P., Ferland, J., and Arrigo, K. R.: Under-ice phytoplankton blooms inhibited by spring convective mixing in
951 refreezing leads, *J Geophys Res Oceans*, 123(1), 90-109, <https://org/10.1002/2016JC012575>, 2018.

952 Lydersen, C., Assmy, P., Falk-Petersen, S., Kohler, J., Kovacs, K. M., Reigstad, M., Stehen, H., Strøm, H., Sundfjord, A.,
953 Varpe, Ø., Walczowski, W., Weslawski, K. M., and Zajaczkowski, M.: The importance of tidewater glaciers for marine
954 mammals and seabirds in Svalbard, Norway, *J Marine Sys*, 129, 452-471, <https://org/10.1016/j.jmarsys.2013.09.006>, 2014.

955 Maes, S.: Polar cod population structure: connectivity in a changing ecosystem, Ph.D. thesis, KU Leuven, Leuven, Belgium,
956 2017.

957 Mahé, F., Rognes, T., Quince, C., de Vargas, C., and Dunthorn, M.: Swarm: robust and fast clustering method for amplicon-
958 based studies, *PeerJ*, 2, e593, <https://org/10.7717/peerj.593>, 2014

959 Massicotte, P., Bécu, G., Lambert-Girard, S., Leymarie, E., and Babin, M.: Estimating underwater light regime under spatially
960 heterogeneous sea ice in the Arctic, *Appl. Sci.*, 8(12), 2693, <https://org/10.3390/app8122693>, 2018.

961 Meire, L., Meire, P., Struyf, E., Krawczyk, D. W., Arendt, K. E., Yde, J. C., Juul Pedersen, T., Hopwood, M. J., Rysgaard, S.,
962 and Meysman, F. J. R.: High export of dissolved silica from the Greenland Ice Sheet, *Geophys. Res. Lett.*, 43, 9173–9182,
963 <https://doi.org/10.1002/2016GL070191>, 2016a.

964 Meire, L., Mortensen, J., Rysgaard, S., Bendtsen, J., Boone, W., Meire, P., and Meysman, F. J.: Spring bloom dynamics in a
965 subarctic fjord influenced by tidewater outlet glaciers (Godthåbsfjord, SW Greenland), *J Geophys Res Biogeosci*, 121(6),
966 1581-1592, <https://org/10.1002/2015JG003240>, 2016b.

967 Meslard, F., Bourrin, F., Many, G., and Kerhervé, P.: Suspended particle dynamics and fluxes in an Arctic fjord (Kongsfjorden,
968 Svalbard), *Estuarine, Estuar Coast Shelf S*, 204, 212-224, <https://org/10.1016/j.ecss.2018.02.020>, 2018.

969 [Mortensen, J., Rysgaard, S., Bendtsen, J., Lennert, K., Kanzow, T., Lund, H., and Meire, L.: Subglacial Discharge and Its](#)
970 [Down-Fjord Transformation in West Greenland Fjords With an Ice Mélange, *J Geophys Res Oceans*, 125\(9\), e2020JC016301,](#)
971 [2020.](#)

972 Moskalik, M., Cwiąkała, J., Szczuciński, W., Dominiczak, A., Głowacki, O., Wojtysiak, K., and Zagórski, P: Spatiotemporal
973 changes in the concentration and composition of suspended particulate matter in front of Hansbreen, a tidewater glacier in
974 Svalbard, *Oceanologia*, 60(4), 446-463 2018.

975 Mock, T., and Gradinger, R.: Determination of Arctic ice algal production with a new in situ incubation technique, *Mar. Ecol.*
976 *Prog. Ser.*, 177, 15-26, <https://org/10.3354/meps177015>, 1999.

977 Molari, M., Manini, E., and Dell'Anno, A.: Dark inorganic carbon fixation sustains the functioning of benthic deep-sea
978 ecosystems, *Global Biogeochem Cycles*, 27(1), 212-221, <https://org/10.1002/gbc.20030>, 2013.

979 Moon, T., Sutherland, D. A., Carroll, D., Felikson, D., Kehrl, L., and Straneo, F.: Subsurface iceberg melt key to Greenland
980 fjord freshwater budget, *Nat Geosci*, 11(1), 49-54, <https://org/10.1038/s41561-017-0018-z>, 2018.

981 Mundy, C. J., Barber, D. G., and Michel, C.: Variability of snow and ice thermal, physical and optical properties pertinent to
982 sea ice algae biomass during spring, *J Marine Sys*, 58(3-4), 107-120, <https://org/10.1016/j.jmarsys.2005.07.003>, 2005.

983 Mundy, C. J., Gosselin, M., Ehn, J., Gratton, Y., Rossnagel, A., Barber, D. G., Martin, J., Tremblay, J., Palmer, M., Arrigo,
984 K. R., Darnis, G., Fortier, L., Else, B., Papakyriakou, T.: Contribution of under-ice primary production to an ice-edge upwelling
985 phytoplankton bloom in the Canadian Beaufort Sea, *Geophys. Res. Lett*, 36(17), <https://org/10.1029/2009GL038837>, 2009.
986 Natural Earth, <http://www.natureearthdata.com/>, last access: 10 August 2020.

987 Norwegian Polar institute, Toposvalbard, <https://toposvalbard.npolar.no>, last access: 16 September 2020.

988 Pabi, S., van Dijken, G. L., and Arrigo, K. R.: Primary production in the Arctic Ocean, 1998–2006, *J Geophys Res Oceans*,
989 113(C8), <https://org/10.1029/2007JC004578>, 2008.

990 Parada, A. E., Needham, D. M., and Fuhrman, J. A.: Every base matters: assessing small subunit rRNA primers for marine
991 microbiomes with mock communities, time series and global field samples, *Environ. Microbiol*, 18(5), 1403-1414,
992 <https://org/10.1111/1462-2920.13023>, 2016.

993 Parsons, T. R., Maita, Y. and Lalli, C. M. (Eds.): *A Manual of Chemical and Biological Methods for Seawater Analysis*.
994 Pergamon Press, Toronto, 1984.

995 Pavlov, A. K., Leu, E., Hanelt, D., Bartsch, I., Karsten, U., Hudson, S. R., Gallet, J., Cottier, F., Cohen, J. H., Berge, J.,
996 Johnsen, G., Maturilli, M., Kowalczyk, P., Sagan, S., Meler, J., and Granskog, M. A.: The underwater light climate in
997 Kongsfjorden and its ecological implications, in: *The Ecosystem of Kongsfjorden, Svalbard*, edited by: Hop, H., and Wiencke,
998 C., Springer, Cham., 137-170, 2019.

999 Perovich, D. K., Roesler, C. S., and Pegau, W. S.: Variability in Arctic sea ice optical properties, *J Geophys Res Oceans*,
1000 103(C1), 1193-1208, <https://org/10.1029/97JC01614>, 1998.

1001 Porter, K. G., and Feig, Y. S.: The use of DAPI for identifying and counting aquatic microflora, *Limnol Oceanogr*, 25, 943–
1002 948, <https://wiley.com/10.4319/lo.1980.25.5.0943>, 1980.

1003 Pruesse, E., Peplies, J., and Glöckner, F. O.: SINA: accurate high-throughput multiple sequence alignment of ribosomal RNA
1004 genes, *Bioinformatics*, 28(14), 1823-1829, 2012.

1005 Ptacnik, R., Andersen, T., and Tamminen, T.: Performance of the Redfield ratio and a family of nutrient limitation indicators
1006 as thresholds for phytoplankton N vs. P limitation, *Ecosystems*, 13(8), 1201-1214, <https://org/10.1007/s10021-010-9380-z>,
1007 2010.

1008 Quast, C., Pruesse, E., Yilmaz, P., Gerken, J., Schweer, T., Yarza, P., Replies, J., and Glöckner, F. O.: The SILVA ribosomal
1009 RNA gene database project: improved data processing and web-based tools. *Nucleic acids research*, 41(D1), D590-D596,
1010 2012.

1011 Redfield, A. C.: On the proportions of organic derivatives in sea water and their relation to the composition of plankton, In
1012 *James Johnstone Memorial Volume*, 176–192. Liverpool University Press, 1934.

1013 Rich, J., Gosselin, M., Sherr, E., Sherr, B., and Kirchman, D. L.: High bacterial production, uptake and concentrations of
1014 dissolved organic matter in the Central Arctic Ocean, *Deep Sea Research Part II: Topical Studies in Oceanography*, 44(8),
1015 1645-1663, 1997.

1016 Sager, J. C., and Mc Farlane, J. C.: Radiation, in: *Plant growth chamber handbook*, edited by: Langhans, R. W., and Tibbits,
1017 T. W., Iowa Agr. Home Econ. Expt. Sta. Special Rpt, 99, 1-29, 1997.

1018 Schaffer, J., and Kanzow, T.: von Appen, W. J.; von Albedyll, L.; Arndt, J. E.; Roberts, D. H. Bathymetry Constrains Ocean
1019 Heat Supply to Greenland's Largest Glacier Tongue, *Nat. Geosci*, 13(3), 227-231, <https://doi.org/10.1038/s41561-019-0529->
1020 [x](https://doi.org/10.1038/s41561-019-0529-x), 2020.

1021 Schoof, C., Rada, C. A., Wilson, N. J., Flowers, G. E., and Haseloff, M.: Oscillatory subglacial drainage in the absence of
1022 surface melt, *The Cryosphere*, 8(3), 959-976, 2014.

1023 Skogseth, R., Olivier, L. L., Nilsen, F., Falck, E., Fraser, N., Tverberg, V., Ledang, A. B., Vader, A., Jonassen, M. O., Søreide,
1024 J., Cottier, F., Berge, J., Ivanov, B. V., and Falk-Petersen, S.: Variability and decadal trends in the Isfjorden (Svalbard) ocean
1025 climate and circulation-an indicator for climate change in the European Arctic, *Prog Oceanogr*, 187, 102394,
1026 <https://org/10.1016/j.pocean.2020.102394>, 2020.

1027 Southwood, T. R. E. and Henderson, P. A. (Eds.): *Ecological methods*, John Wiley and Sons, 269, 2000.

1028 Strzelecki, M. C.: Schmidt hammer tests across a recently deglaciated rocky coastal zone in Spitsbergen-is there a "coastal
1029 amplification" of rock weathering in polar climates?, *Pol Polar Res*, 239-252, <https://org/10.2478/v10183-011-0017-5>, 2011.

1030 Sutherland, D. A., Pickart, R. S., Peter Jones, E., Azetsu-Scott, K., Jane Eert, A., and Ólafsson, J.: Freshwater composition of
1031 the waters off southeast Greenland and their link to the Arctic Ocean, *J Geophys Res Oceans*, 114(C5),
1032 <https://org/10.1029/2008JC004808>, 2009.

1033 Sutherland, D. A., Straneo, F., & Pickart, R. S.: Characteristics and dynamics of two major Greenland glacial fjords, *Journal*
1034 *of Geophysical Research: Oceans*, 119(6), 3767-3791, 2014.

1035 Throndsen, J., Hasle, G. R., & Tangen, K. (Eds.): *Phytoplankton of Norwegian coastal waters*, Almater Forlag AS, 2007.

1036 Tomas, C. R. (Ed.): *Identifying Marine Phytoplankton*, Elsevier, San Diego, 1997.

1037 Utermöhl, H.: Methods of collecting plankton for various purposes are discussed, *SIL Commun* 1953-1996. 9, 1-38,
1038 <https://doi.org/10.1080/05384680.1958.11904091>, 1958.

1039 Van De Poll, W. H.; Kulk, G.; Rozema, P. D.; Brussaard, C. P. D.; Visser, R. J. W.; Buma, A. G. J. Contrasting Glacial
1040 Meltwater Effects on Post-Bloom Phytoplankton on Temporal and Spatial Scales in Kongsfjorden, Spitsbergen, *Elementa*,
1041 <https://doi.org/10.1525/elementa.307>, 2018.

1042 Vihtakari, M.: PlotSvalbard: PlotSvalbard - Plot research data from Svalbard on maps. R package version 0.9.2,
1043 <https://github.com/MikkoVihtakari/PlotSvalbard>, 2020.

1044 von Quillfeldt, C. H.: Common diatom species in Arctic spring blooms: their distribution and abundance, *Bot Mar*, 43(6), 499-
1045 516, <https://org/10.1515/BOT.2000.050>, 2000.

1046 von Quillfeldt, C. H., Ambrose, W. G., and Clough, L. M.: High number of diatom species in first-year ice from the Chukchi
1047 Sea, *Polar Biol*, 26(12), 806-818, <https://org/10.1007/s00300-003-0549-1>, 2003.

1048 Vonnahme, T. R., Devetter, M., Žárský, J. D., Šabacká, M., and Elster, J.: Controls on microalgal community structures in
1049 cryoconite holes upon high Arctic glaciers, Svalbard, *Biogeosciences*, 13, 659-674, <https://org/10.5194/bg-13-659-2016>, 2016.

1050 Wadhwa, J. L., Hodgkins, R., Cooper, R. J., and Tranter, M.: Evidence for seasonal subglacial outburst events at a polythermal
1051 glacier, Finsterwalderbreen, Svalbard, *Hydrol. Process.*, 15(12), 2259-2280, <https://org/10.1002/hyp.178>, 2001.

1052 Wang, Q., Garrity, G. M., Tiedje, J. M., and Cole, J. R.: Naive Bayesian Classifier for Rapid Assignment of rRNA Sequences
1053 into the New Bacterial Taxonomy, *Appl Environ Microbiol.* 73(16), 5261-7, <https://org/10.1128/AEM.00062-07>, 2007.

1054 Wangenstein, O. S., Palacín, C., Guardiola, M., and Turon, X.: DNA metabarcoding of littoral hard-bottom communities: high
1055 diversity and database gaps revealed by two molecular markers, *PeerJ*, 6, e4705, <https://org/10.7717/peerj.4705>, 2018.

1056 Wiedmann, I., Reigstad, M., Marquardt, M., Vader, A., and Gabrielsen, T. M.: Seasonality of vertical flux and sinking particle
1057 characteristics in an ice-free high arctic fjord—Different from subarctic fjords?, *J Marine Sys*, 154, 192-205,
1058 <https://org/10.1016/j.jmarsys.2015.10.003>, 2016.

1059 Wilson, N.: Characterization and interpretation of polythermal structure in two subarctic glaciers, Doctoral dissertation,
1060 Science: Department of Earth Sciences, 2012.

1061 Wynn, P. M., Hodson, A. J., Heaton, T. H., and Chenery, S. R.: Nitrate production beneath a High Arctic glacier, Svalbard,
1062 *Chemical geology*, 244(1-2), 88-102, 2007.

1063 yr.no, Longyearbyen – historikk, [https://www.yr.no/nb/historikk/graf/1-](https://www.yr.no/nb/historikk/graf/1-2759929/Norge/Svalbard/Svalbard/Longyearbyen?q=2019-04)
1064 [2759929/Norge/Svalbard/Svalbard/Longyearbyen?q=2019-04](https://www.yr.no/nb/historikk/graf/1-2759929/Norge/Svalbard/Svalbard/Longyearbyen?q=2019-04), last access: 24 July 2020.

1065
1066
1067
1068
1069
1070
1071
1072
1073
1074
1075
1076
1077
1078
1079

1080

1081

1082

1083

1084

1085

1086

1087

1088

1089

1090

1091

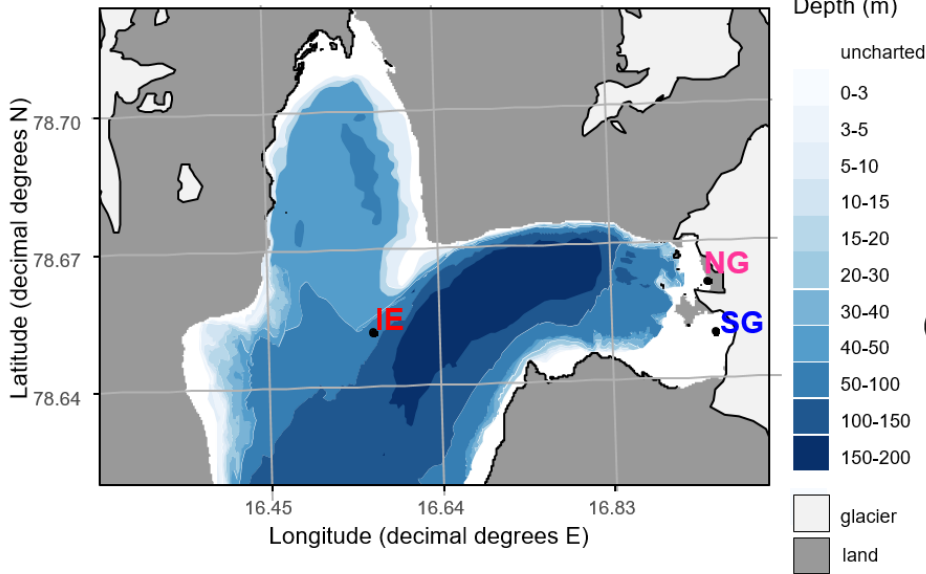
1092

1093

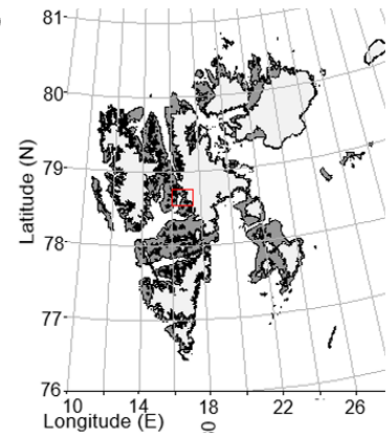
1094 **Figures**

1095

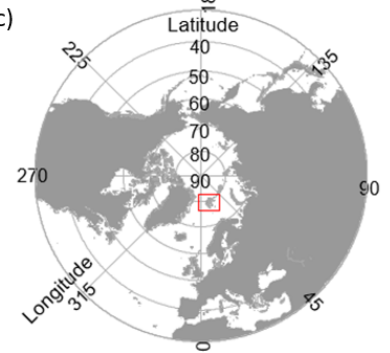
(a)



(b)



(c)

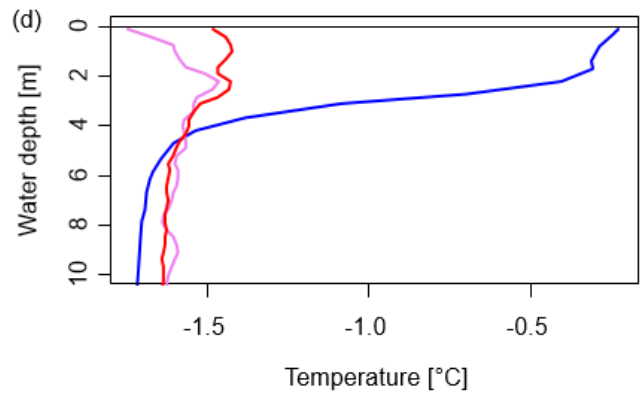
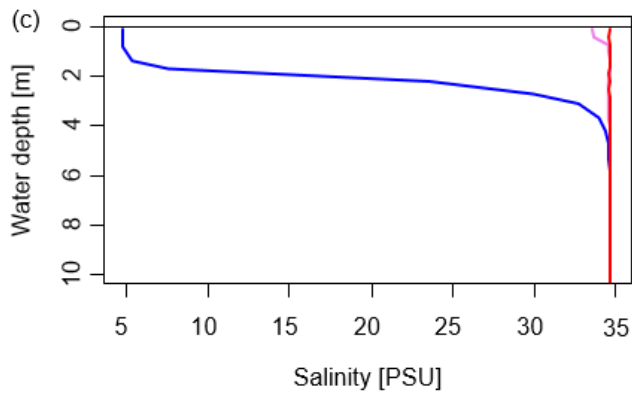
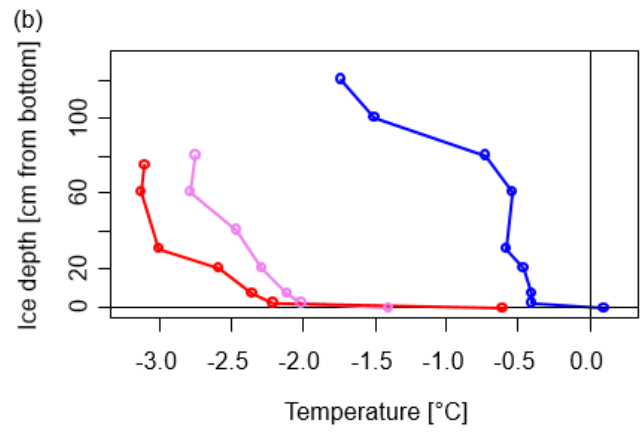
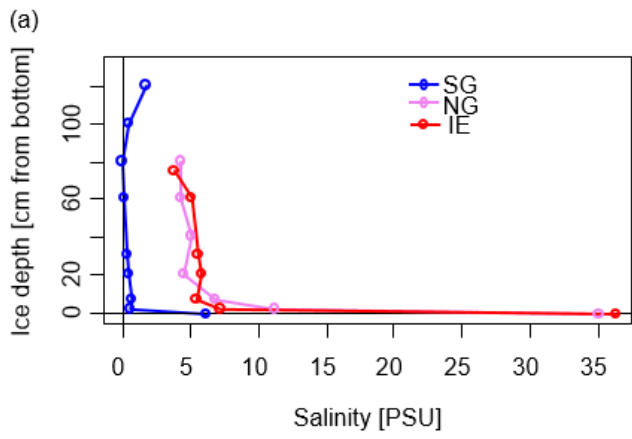


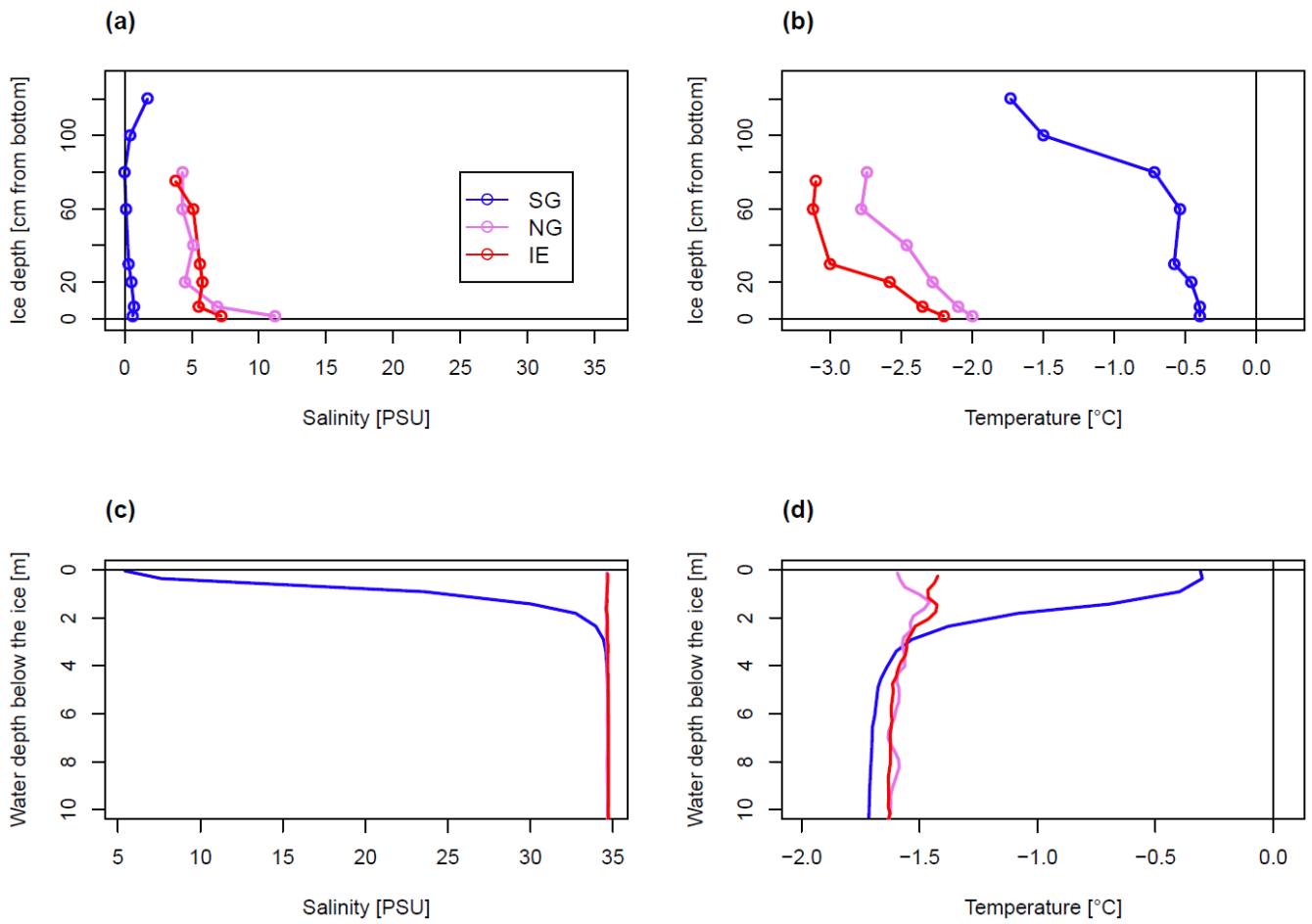
1096

1097 Fig 1. Sampling sites in Billefjorden: a) detailed Billefjorden map showing the stations at the ice edge (IE), north glacier (NG)
1098 and south glacier (SG) on the underlying bathymetric map. White areas are uncharted with water depths of about 30 m at NG
1099 and SG. The insets to the right show the location of b) Billefjorden on a Svalbard map and of c) Svalbard on a pan-Arctic map,
1100 marked with red boxes. Land is shown as dark grey, ocean as white, and glaciers as light grey. All maps were created using
1101 the PlotSvalbard R package (Vithakari, 2019). The Svalbard basemap is retrieved from the Norwegian Polar institute (2020,
1102 CC BY 4.0 license), the pan-Arctic map is retrieved from Natural Earth (2020, CC Public domain license), and the bathymetric
1103 map is retrieved from the Norwegian mapping authority (Kartverket, 2020, CC BY 4.0 license).

1104

1105





1107

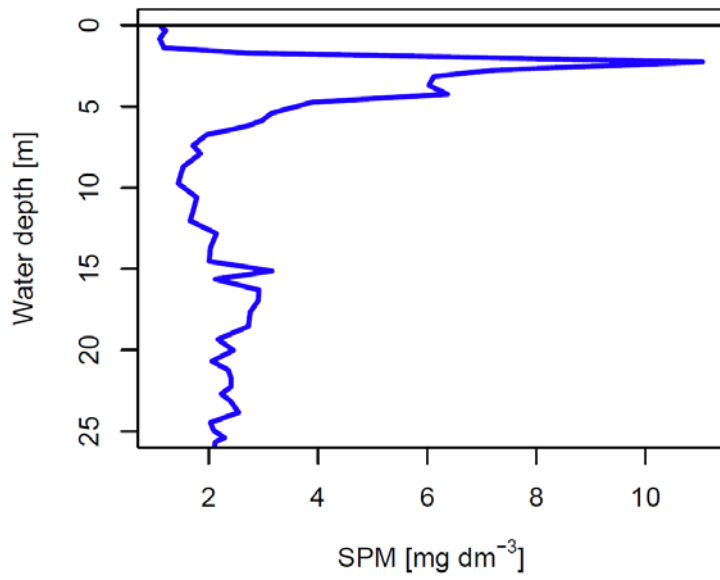
1108 Fig 2. Bulk salinity and temperature profiles in a,b) sea ice cores (0 cm at the bottom) and c,d) the water column down to 10
 1109 m below the sea ice, of the three stations.

1110

1111

1112

1113



1114

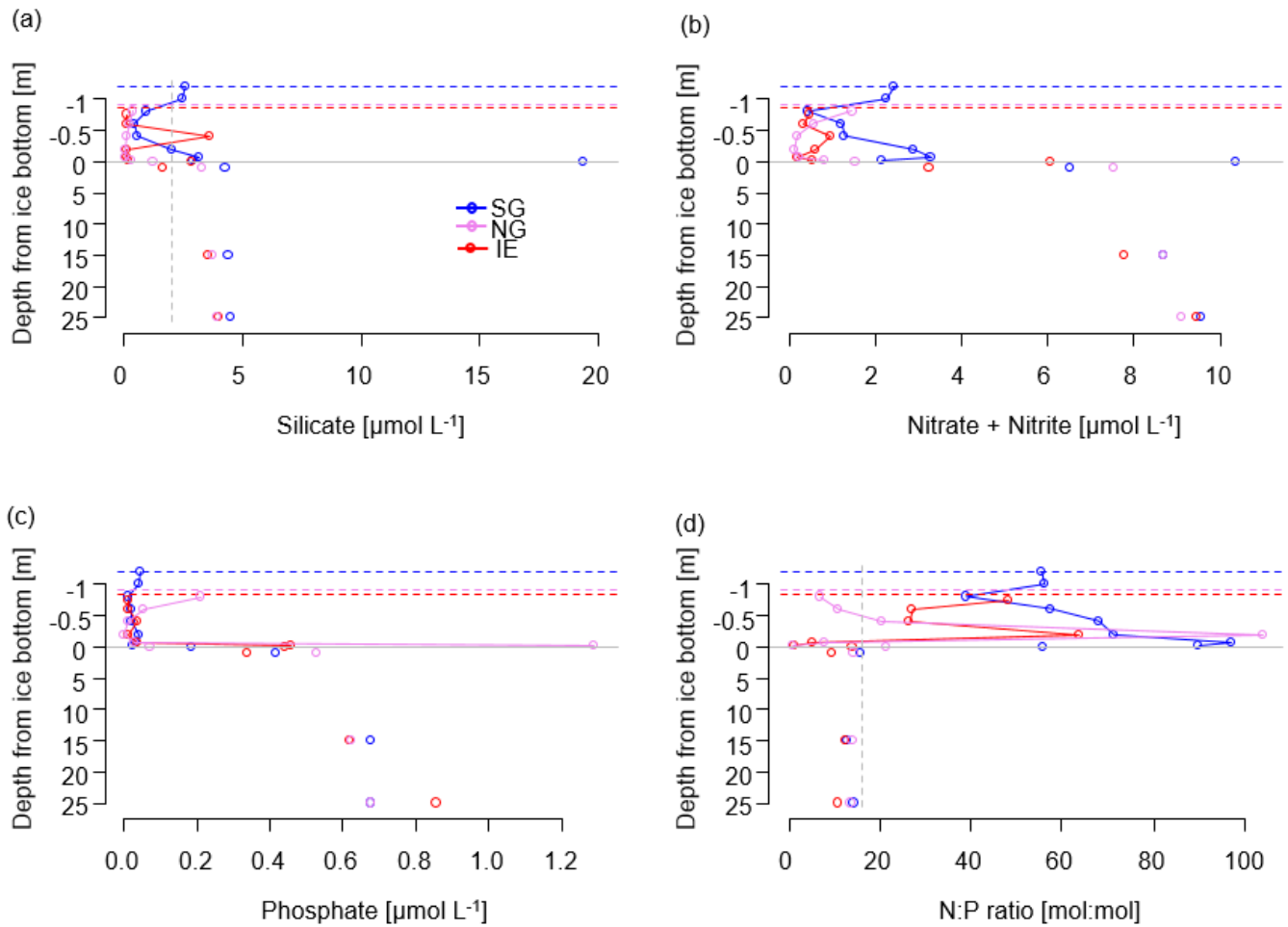
1115 Fig 3. Turbidity profile of the SG station converted to suspended particles.

1116

1117

1118

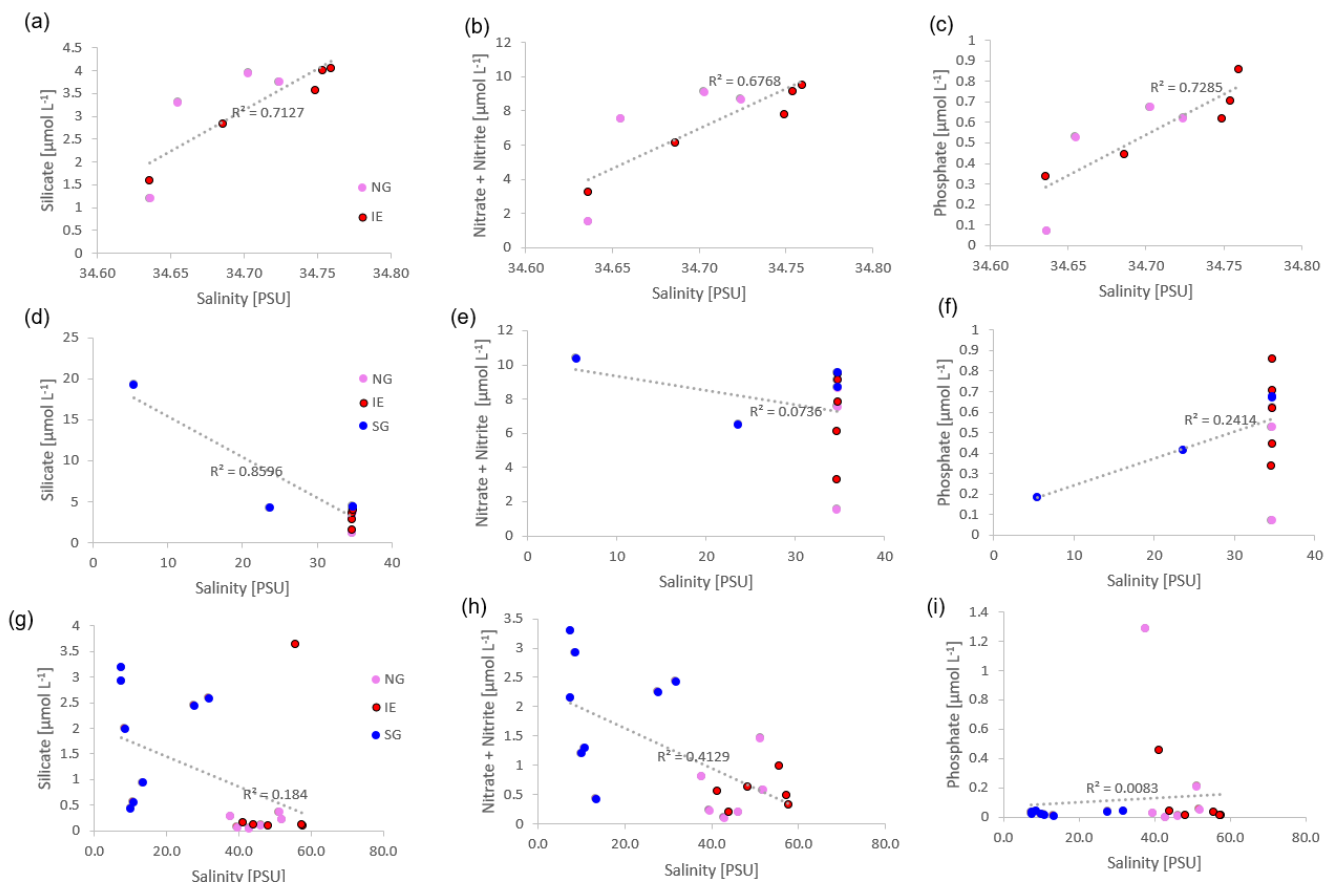
1119

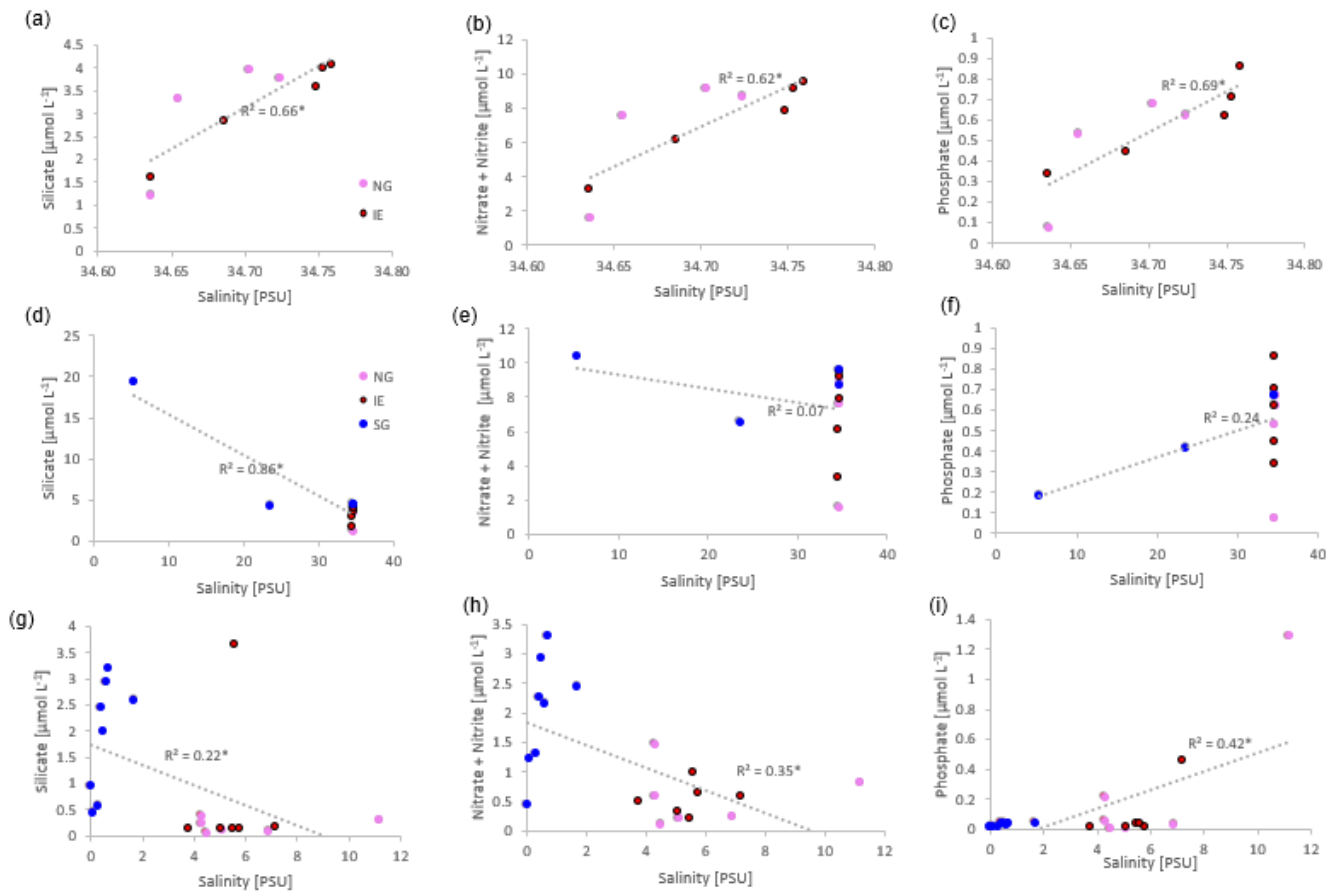


1120

1121 Fig 4. Nutrient concentrations Nutrients in the water column (below grey line) and in sea ice (above the grey line) of a) silicate
 1122 with a suggested threshold for limitation marked as dashed grey line, b) NO_x as nitrate and nitrite, c) phosphate and d) molar
 1123 N:P ratios with the Redfield threshold of N:P 16:1 marked as dashed grey line indicating potential N limitation. Dashed lines
 1124 indicate the position of the ice surface, while solid lines show the measured data.

1125

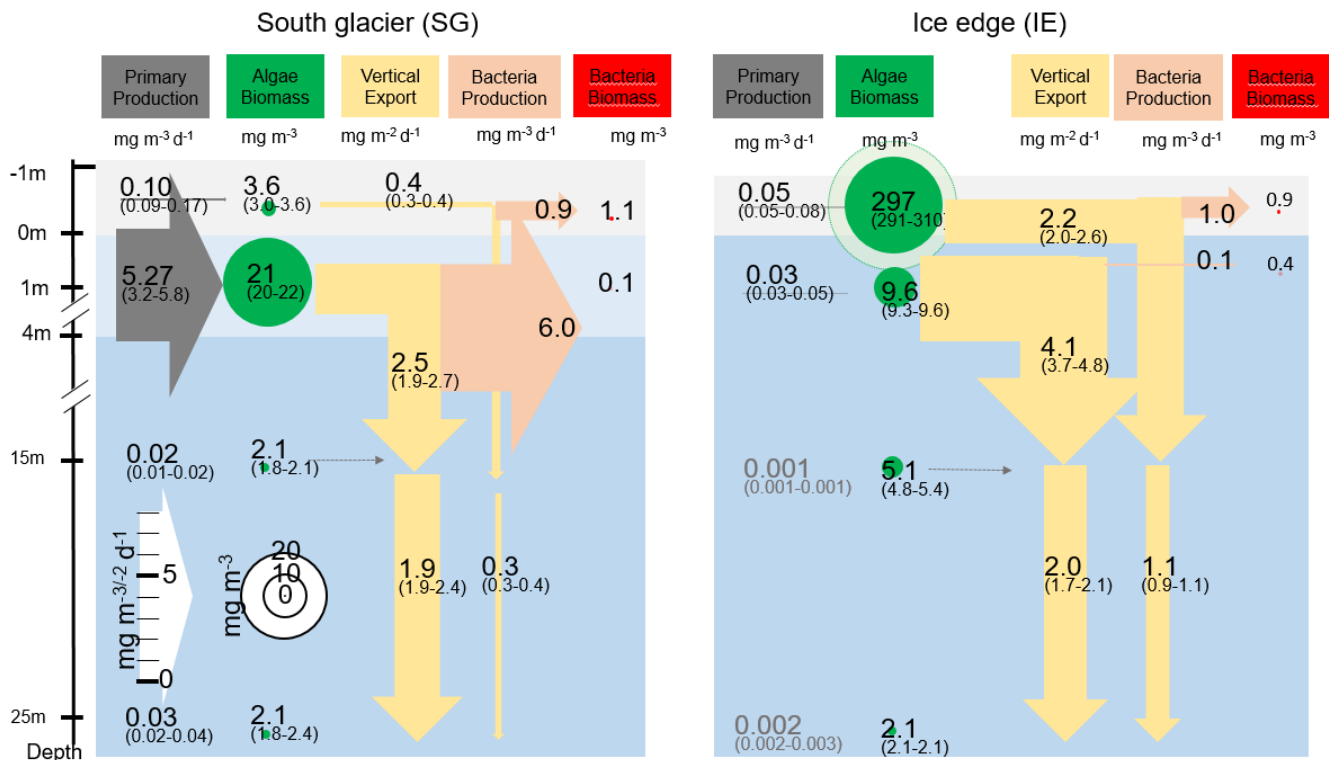




1128

1129 Fig 5. Linear salinity-nutrient correlations of NG and IE water samples (a–c), NG, IE, and SG water stations (d–f) and sea ice
 1130 samples of NG, IE and SG (bulk salinities) (g–i). A higher concentration in saline Atlantic water is shown as a positive
 1131 correlation, a higher concentration in glacial meltwater as a negative correlation. Significant correlations ($p < 0.05$) are asterisk
 1132 marked behind the R^2 value.

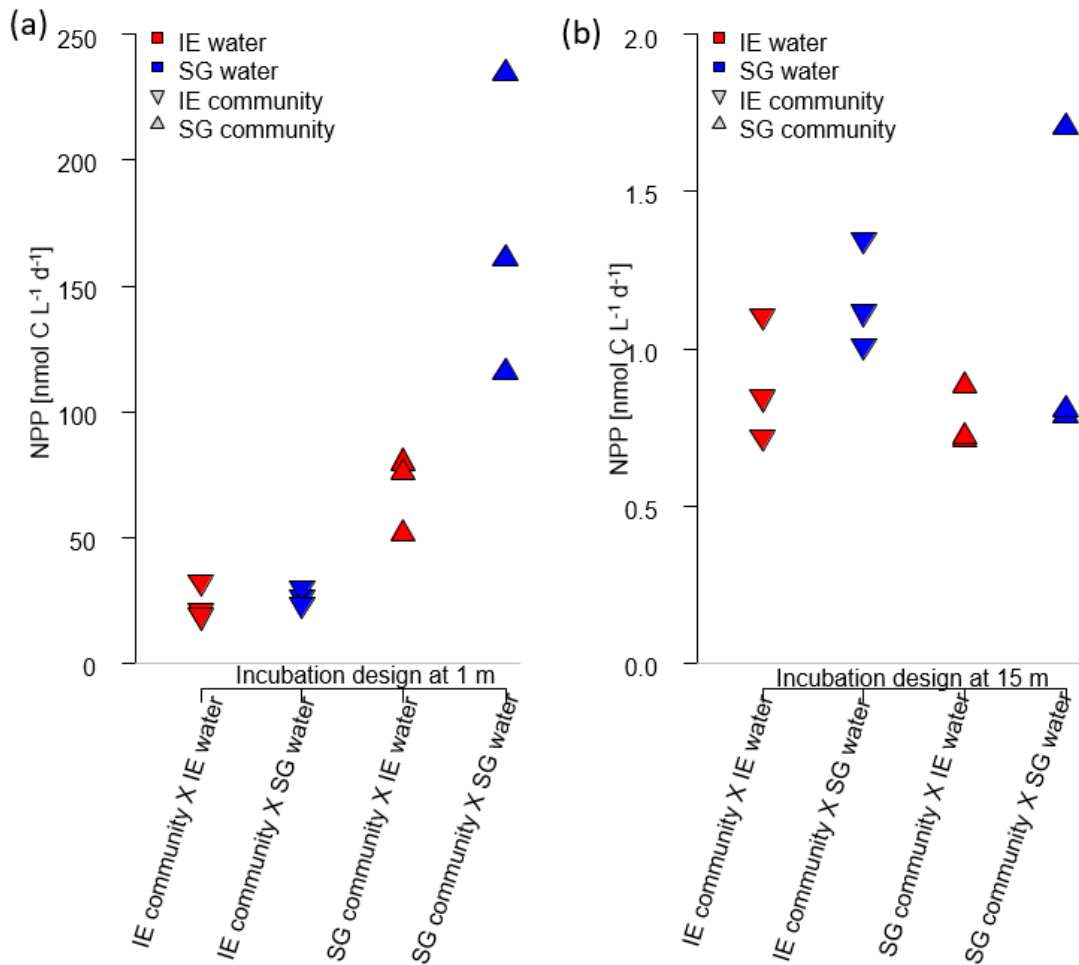
1133



1135

1136 Fig 6. Schematic representation of the C cycle at SG and IE stations. All units are in mg C with the median given in the circles
 1137 and arrows and the minimum and maximum in brackets below. 0 m depth is at the sea ice water interface. Grey arrows indicate
 1138 net primary production with its height scaled to the uptake rates. Green circles show standing stock algae biomass converted
 1139 from Chl to C (conversion factor = 30 gC gChl⁻¹, Cloern et al., 1995) with its diameter scaled to the concentrations, except sea
 1140 ice at IE with the light green circle scaled one order of magnitude higher. Yellow arrows indicate vertical export of chlorophyll
 1141 converted to C (conversion factor = 30 gC gChl⁻¹, Cloern et al., 1995) with the contribution of sea ice algae and phytoplankton
 1142 estimated by the fraction of typical sea ice algae in phytoplankton net hauls and the width of the arrows scaled to the fluxes.
 1143 Orange arrows indicate bacterial biomass production based on dark carbon fixation (conversion factor = 129 gC gDIC⁻¹, Molari
 1144 et al., 2013) with the arrows scaled to the values. Red circles to the right are bacteria biomass assuming 20 fg C cell⁻¹ in the
 1145 bottom sea ice and UIW. The grey area represents sea ice, the light blue area a brackish water layer and the darker blue area
 1146 deeper saline water layers.

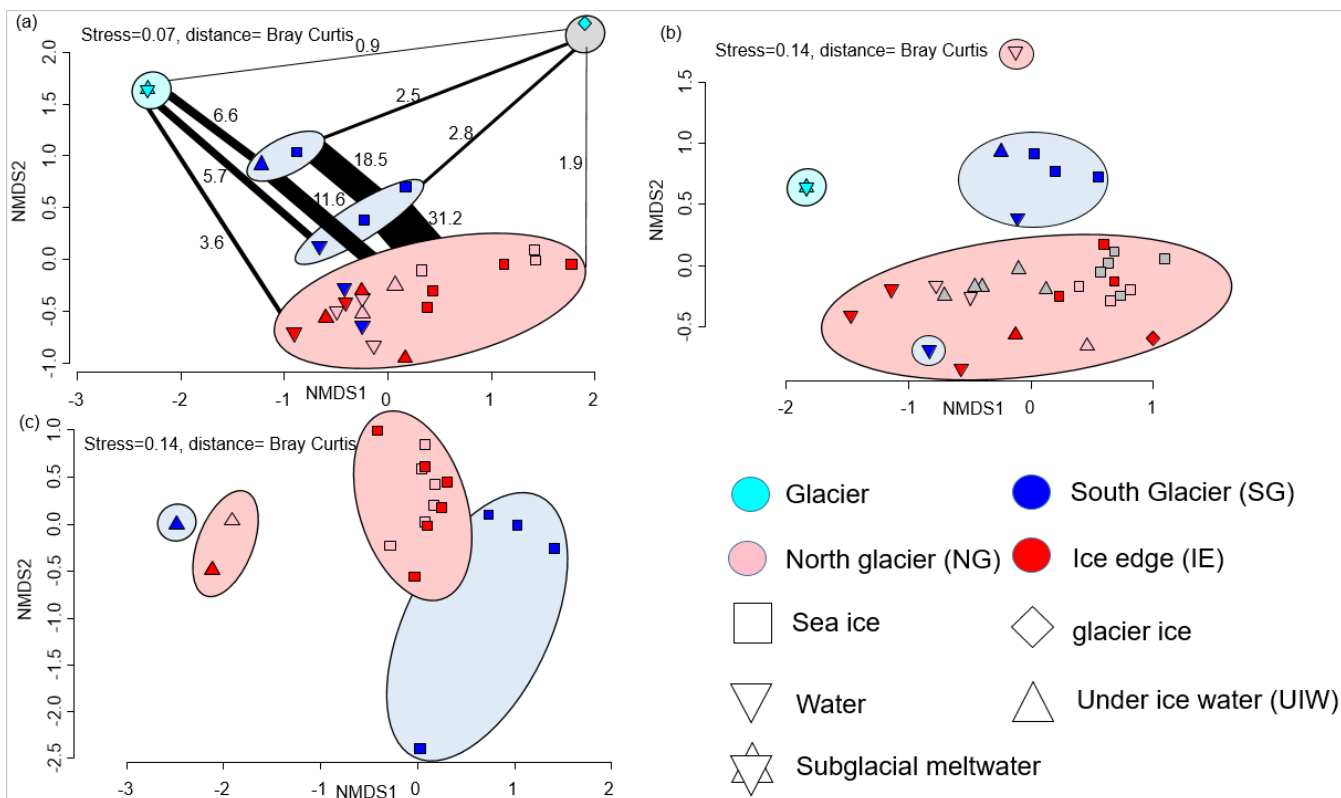
1147



1148

1149 Fig 7. Impact of water source on primary production assessed via a reciprocal transplant experiment. Primary production of
 1150 IE and SG communities incubated in sterile filtered water originated from either station at a) 1 m and b) 15 m depth. The
 1151 symbols show the source of the community and the colors indicate the source of the sterile filtered incubation water. The type
 1152 of incubation water (color) explains the variation in a nested ANOVA with community (symbol) and depth as nested
 1153 constrained variables and water source (color) as explanatory variable ($p=0.0038$, $F=10.88$).

1154



1156

1157 Fig 8. a) NMDS plot of microbial community structure based on 16S data (stress = 0.07), including samples from April 2018.
 1158 Groups highlighted in eclipses: glacier ice (top right in grey eclipse), undiluted subglacial outflow (top left in cyan eclipse),
 1159 surface samples (UIW, sea ice) at station SG 2019 (top blue eclipse), surface samples (1m water, sea ice) at station SG 2018
 1160 (bottom blue eclipse) and others including deeper water samples at SG (bottom in red eclipse). The fraction of shared OTUs
 1161 (in %) are shown as lines scaled to the fraction [%] of shared OTUs. b) NMDS plot of community structure based on 18S data
 1162 (stress = 0.14), including samples from April 2018 with the surface water sample of NG as outlier on top, and a surface water
 1163 sample of SG as outlier in the pink reference cluster, c) NMDS plot based on algae abundances in sea ice and UIW based on
 1164 light microscopic counts (stress = 0.14).

1165

1166

1167

1168

1169

1170

1171

1172 **Tables**

1173 Table 1. Properties of 1) marine surface and 2) Marine deep water (both station IE), 3) subglacial discharge melt water and 4)
 1174 station SG surface water and the relative contribution of the water types 1 to 3 to form water type 4. The calculations are given
 1175 in the Supplement and are based on different salinities and nutrients in the 4 water masses.

	1) Surface water (IE 1 m)		2) Bottom water (IE)		3) Subglacial discharge Meltwater		4) SG (1 m)
Salinity [PSU]	34.7		34.7		0 32 ± 0.1 %		23.6
Temperature [°C]	-1.4		-1.4		0		-0.4
Silicate [$\mu\text{mol L}^{-1}$]	1.59	0 %	4.46	> 84 %	1.79	32 %	4.30
NO _x [$\mu\text{mol L}^{-1}$]	3.27	10 ± 3 %	9.57	58 ± 1 %	2.06	32 %	6.52
Phosphate [$\mu\text{mol L}^{-1}$]	0.34	19 ± 3 %	0.67	49 ± 3 %	0.09	32 %	0.42

1176

1177

1178

1179

1180

1181

1182

1183

1184

1185

1186

1187

1188

1189

1190

1191

1192

1193

1194

1195

1196

1197 Table 2. Integrated standing stock biomass of Chl and fluxes of Chl and C, fractions of the different fluxes and standing stocks,
 1198 and bacterial production based on dark carbon fixation (DCF).

Variable	SG	IE	Unit
Chl int. integrated in sea ice	0.02	0.40	mg m ⁻²
NPP in bottom sea ice	0.10	0.05	mg C m ⁻³ d ⁻¹
Chl int. integrated in 25 m water column	3.74	3.75	mg m ⁻²
Vertical Chl flux to 25 m	0.07	0.11	mg Chl m ⁻² d ⁻¹
NPP at 1 m	5.27	0.03	mg C m ⁻³ d ⁻¹
C based NPP int. over 25 m	42.6	0.2	mg C m ⁻² d ⁻¹
Estimated Chl production int. over 25 m	1.4	0.0	mg C m ⁻² d ⁻¹
mg C fixed per mg Chl	11.4	0.1	mg C mg Chl d ⁻¹
NPP as fraction of Chl standing stock	38 %	0.2 %	% Chl renewal d ⁻¹
Doubling time	2.63	500	days
Vertical Chl flux as % of Chl standing stock	2 %	3 %	% export of Chl d ⁻¹
Vertical Chl flux as % of NPP based Chl prod.	5 %	1375 %	% export of NPP d ⁻¹
Loss of Chl from 15 to 25 m	12 %	19 %	Δexp 15m to 25m
Average Chl fraction of (Chl + Phaeo) in 0-3 cm ice	30%	85%	% Chl
Average Chl fraction of (Chl + Phaeo) in water	47 %	50 %	% Chl
Bacteria DCF ice	7.0	7.6	μg C m ⁻³ d ⁻¹
Bacteria Biomass prod (DCF based) ice	0.9	1.0	mg C m ⁻³ d ⁻¹
Doubling time	1.2	0.9	days
Bacteria DCF 1 m	46.9	1.1	μg DIC m ⁻³ d ⁻¹
Bacteria Biomass prod (DCF based) 1m	6.0	0.1	mg C m ⁻³ d ⁻¹
Doubling time	0.02	2.9	days

1199

1200

1201

1202

1203

1204

1205

1206

1207

1208 **Appendix**

1209 Equations 1-6. Mixing calculations for estimates of the fraction of meltwater (MW_{Sal}) based on salinity, and for bottom water
 1210 based on nutrient concentrations (BW_{Nuts}). Sal indicates the average salinities measured at the IE (Sal_{IE}), SG at 1m depth
 1211 (Sal_{SG1m}), subglacial outflow (Sal_{glac}). Nut indicates the nutrient concentrations of nitrate and nitrite (NO_x), silicate (Si), and
 1212 phosphate (PO_4) at 1m under the sea ice at SG (Nut_{1mSG}) and IE (Nut_{1mIE}), the bottom water of the IE (Nut_{BW}), or subglacial
 1213 outflow water (Nut_{glac}).
 1214

$$1215 \quad MW_{Sal}[\%] = \frac{Sal_{IE} - Sal_{SG1m}}{Sal_{SG1m} - Sal_{glac} + Sal_{IE} - Sal_{SG1m}} * 100 \quad (1)$$

$$1216 \quad MW_{Sal}[\%] = \frac{34.7 \text{ PSU} - 23.6 \text{ PSU}}{23.6 \text{ PSU} - 0 \text{ PSU} + 34.7 \text{ PSU} - 23.6 \text{ PSU}} * 100 = 32 \% \quad (2)$$

$$1217 \quad BW_{Nut}[\%] = \frac{Nut_{1mSG} - MW_{Sal}[\%] * Nut_{glac} - Nut_{1mIE} + MW_{Sal}[\%] * Nut_{1mIE}}{Nut_{BW} - Nut_{1mIE}} * 100 \quad (3)$$

$$1218 \quad BW_{NOx}[\%] = \frac{6.52 \mu M - 0.32 * 2.06 \mu M - 3.27 \mu M + 0.32 * 3.27 \mu M}{9.57 \mu M - 3.27 \mu M} * 100 = 58 \% \quad (4)$$

$$1219 \quad BW_{Si}[\%] = \frac{4.30 \mu M - 0.32 * 1.79 \mu M - 1.59 \mu M + 0.32 * 1.59 \mu M}{4.46 \mu M - 1.59 \mu M} * 100 = 92 \% \quad (5)$$

$$1220 \quad BW_{PO4}[\%] = \frac{0.41 \mu M - 0.32 * 0.09 \mu M - 0.34 \mu M + 0.32 * 0.34 \mu M}{0.67 \mu M - 0.34 \mu M} * 100 = 46 \% \quad (6)$$

1225

1226

1227 Equation 7. Calculation of vertical flux ~~eg-of~~ Chl based on the sediment traps with concentration of Chl (C), Volume in the
 1228 sediment trap cylinder (V), area above the cylinder (A) and incubation time (t).

$$1229 \quad \text{Vertical flux} = \frac{C * V}{A * t} \quad (7)$$

1230

1231

1232

1233

1234

1235

1236

1237

1238

1239

1240

1241